

Complex Absorbing Potential Green's Function Methods for Resonances

Loris Burth, Fábris Kossoski, and Pierre-François Loos*



Cite This: *J. Chem. Theory Comput.* 2025, 21, 11463–11480



Read Online

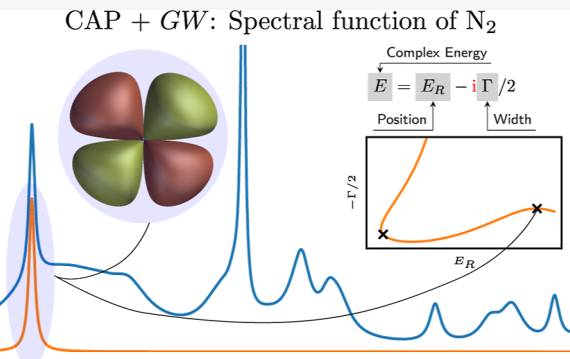
ACCESS |

Metrics & More

Article Recommendations

Supporting Information

ABSTRACT: The complex absorbing potential (CAP) formalism has been successfully employed in various wave function-based methods to study electronic resonance states. In contrast, Green's function-based methods are widely used to compute ionization potentials and electron affinities but, despite a few influential contributions, have seen only limited application to resonances. We integrate the CAP formalism within the *GW* approximation, enabling the description of electronic resonances in a Green's function framework. This approach entails a fully complex treatment of orbitals and quasiparticle energies in a non-Hermitian setting. We validate our CAP-*GW* implementation by applying it to the prototypical shape resonances of N_2^- , CO^- , CO_2^- , C_2H_2^- , C_2H_4^- , and CH_2O^- . It offers a fast and practical route to approximate both the lifetimes and positions of resonance states, achieving an accuracy comparable to that of state-of-the-art wave function-based methods.



1. INTRODUCTION

Anions can be classified as either electronically bound or unbound, based on the sign of the electron affinity (EA) of their corresponding neutral parent state.^{1–7} Bound anions, characterized by positive EAs, can accommodate an additional electron in a square-integrable state. Two subclasses exist. In valence-bound anions, an additional electron occupies a π^* or σ^* antibonding orbital. As a notable example, the C_2 molecule possesses a negative lowest-unoccupied molecular orbital (LUMO) energy and can thus bind an additional electron. Valence-bound anions are even more prevalent in large π -conjugated systems, such as DNA, where low-energy electron attachment (0.1–0.2 eV) can weaken chemical bonds and lead to single- or double-strand breaks.^{8–11} In dipole-bound anions (like NC-CH_3^- or NCH^-), the extra electron resides in an extremely diffuse orbital stabilized by the long-range electric field of a permanent dipole moment (typically $\mu \geq 2.5 \text{ D}$).^{2,3} Here, the electron remains far from the molecular core, and the binding energy is very small, often between a few meV to a few hundred meV. Such dipole-bound states are ubiquitous in water clusters, where the cumulative dipole moment is sufficient to weakly bind an electron.¹²

In contrast to bound anions, unbound anions possess negative EAs.^{7,13} These anions are therefore temporary, corresponding to metastable electronic resonances, that is, discrete states embedded within the continuum that decay via electron autodetachment. Unlike bound states, which have real-valued energies, resonances are characterized by a complex (Gamow–Siegert) energy^{14,15}

$$E = E_R - i\Gamma/2 \quad (1)$$

where E_R denotes the resonance position and Γ is the resonance width, which is related to the lifetime against autoionization by \hbar/Γ .¹⁶ In the inner molecular region, these so-called Gamow–Siegert states exhibit a large amplitude similar to that of bound states. However, in the asymptotic region, their wave functions oscillate like those of unbound states. The complex energy leads to an exponential decay in time of the state's amplitude, reflecting its metastable character. As a result, these states are not square-integrable, and standard Hermitian methods are inapplicable (see below).

Resonances are typically classified into two families. Shape resonances involve a one-electron decay process in which the excess electron is temporarily trapped in an antibonding orbital. Typical examples are the Π -shape resonances of N_2^- and CO^- , or electronically excited states of closed-shell anions.^{17–19} Feshbach resonances,^{20–25} in contrast, occur when electron attachment is accompanied by an internal electronic excitation of the molecule, resulting in a two-electron transition for detachment. A well-known example is the doubly excited ${}^1\Sigma_g^+$ state of H_2 .^{26,27} This added complexity confers longer lifetimes, often extending to the microsecond

Received: July 15, 2025

Revised: October 22, 2025

Accepted: October 22, 2025

Published: November 8, 2025



range, and gives rise to much narrower spectral features. In systems such as the *para*-benzoquinone radical anion, both shape and Feshbach resonances manifest simultaneously.^{19,28–32}

Temporary anions can form either by direct electron attachment to a neutral molecule or via photoexcitation of a bound anion. With lifetimes ranging from tens of femtoseconds to a few picoseconds, they appear spectroscopically as broadened peaks and play important roles in diverse processes, including radiation-induced DNA damage,^{8–11} radiosensitization,³³ interstellar chemistry,³⁴ and nanofabrication.^{35,36} Other types of resonances include multiply charged anions, core-excited and core-ionized states, superexcited states, and Stark resonances.^{37,38}

Because temporary anion wave functions exhibit both bound and continuum character, they are not square integrable and require non-Hermitian theoretical treatments. A widely used approach is the complex absorbing potential (CAP) method,^{39–47} in which a complex potential is added to the Hamiltonian to absorb the resonance tail, rendering the state square integrable. This allows resonances to be treated analogously to bound states, enabling the computation of their positions and widths with adapted quantum chemistry methods.

As with other non-Hermitian approaches, such as complex scaling^{48,49} or the use of complex basis functions,^{50,51} the CAP-modified Hamiltonian becomes complex-valued and non-Hermitian.^{37,38,52} Consequently, resonances emerge directly as eigenstates of this modified Hamiltonian, each characterized by a complex energy whose imaginary part encodes the resonance width.

The CAP formalism must be coupled with a specific electronic structure method. It has been successfully combined with a broad range of wave function- and density-based approaches. These include selected configuration interaction (SCI),⁵³ equation-of-motion electron-attached coupled-cluster with singles and doubles (EOM-EA-CCSD),^{42,43,54} Fock-space multireference coupled-cluster theory,^{55,56} coupled-cluster with perturbative triples,^{57,58} symmetry-adapted-cluster configuration interaction,⁵⁹ extended multiconfigurational quasidegenerate second-order perturbation theory (XMCQDPT2),^{30,60} multireference configuration interaction (MRCI),^{41,61} and density-functional theory (DFT).⁶² In addition, alternative implementations of some of these methods exist, where the CAP-augmented Hamiltonian is projected onto a subspace spanned by a finite number of eigenstates of the physical Hamiltonian. A notable example is the “projected” CAP-EOM-CCSD approach.⁶³

However, studies involving Green’s function methods in this context remain rather limited. A notable exception is the work of Cederbaum and co-workers, who explored the combination of CAP with the second-order algebraic diagrammatic construction (ADC). More recently, the third-order ADC approach was applied to paradigmatic resonances^{67,68} thanks to the development of the intermediate state representation (ISR) formalism, which allows for the decoupling of the ionization potential (IP) and EA sectors via the so-called non-Dyson framework.^{69,70}

Within the broad family of Green’s function methods,^{71–73} the GW approximation^{74–76} has, to the best of our knowledge, been applied to unbound anions only once.⁷⁷ In that study, the authors combined GW with the stabilization method by scaling the exponents of the most diffuse basis functions, then

analytically continued the computed energies into the complex plane. This general framework can be applied to any electronic structure method.⁷⁸

This is somewhat surprising, given that GW is known to perform very well for valence^{79–85} and core^{86–92} IPs in molecules. In fact, the accuracy of GW is such that designing effective beyond-GW schemes that outperform it at a reasonable computational cost remains a significant challenge.^{93–116} Importantly, algorithmic improvements have been designed to lower the computational scaling of GW, which can thus be applied to very large systems.^{87,92,117–133} However, its performance for anions, particularly unbound ones, is much less well-documented. Although some benchmark studies exist for bound anions,^{79,80,114,116,129,134–138} we are not aware of any investigations addressing unbound anions using the standard non-Hermitian frameworks, such as CAP, complex scaling, or complex basis functions.

We also note the recent work of Ghosal, Joshi, and Voora,¹³⁹ who developed a scheme based on exact exchange (EXX) and a random-phase approximation (RPA) correlation functional within a generalized Kohn–Sham framework. By incorporating nonlocal exchange and long-range polarization effects through RPA, their approach yields more reliable molecular electron affinities than standard Kohn–Sham schemes. While this method may be regarded as Green’s function-inspired due to its use of the RPA functional, it does not explicitly rely on the one-body Green’s function.

The goal of the present study is to introduce the CAP-GW approach and evaluate its performance in describing shape resonances. To this end, we investigate different levels of GW self-consistency: (i) the widely used one-shot scheme, known as G_0W_0 ,^{140–146} (ii) the eigenvalue self-consistent GW (evGW) method, in which self-consistency is enforced on the quasiparticle energies,^{137,147–150} and (iii) the quasiparticle self-consistent GW (qsGW) scheme, which extends self-consistency to both the energies and orbitals.^{128,151–157} Calculations are performed for six widely studied shape resonances in small molecules, and the resulting resonance parameters are compared against available experimental data and CAP-augmented state-of-the-art theoretical approaches, namely, CAP-SCI and CAP-EOM-EA-CCSD.

2. THEORY

2.1. Complex Absorbing Potential. When dealing with resonance states, the wave function exhibits an oscillating, nondecaying tail that prevents it from being square-integrable. To address this, a CAP is introduced into the electronic Hamiltonian. Specifically, a term $-i\eta\hat{W}$, with $\eta > 0$, is added to the original N -electron Hamiltonian \hat{H} , leading to the modified Hamiltonian

$$\hat{H}(\eta) = \hat{H} - i\eta\hat{W} \quad (2)$$

where \hat{W} is defined as a sum of one-electron contributions

$$\hat{W} = \sum_{k=1}^N \hat{w}_k \quad (3)$$

The one-body potential \hat{w}_k can take various forms, but the most commonly employed choice is a quadratic form

$$\hat{w}_{\alpha_k} = \begin{cases} (|\alpha_k| - \alpha_0)^2 & \text{if } |\alpha_k| > \alpha_0 \\ 0 & \text{otherwise} \end{cases} \quad (4)$$

Here $\hat{w}_k = \hat{w}_{x_k} + \hat{w}_{y_k} + \hat{w}_{z_k}$ sums over the Cartesian components $\alpha_k \in \{x_k, y_k, z_k\}$ of the k th electron, and $\alpha_0 \in \{x_0, y_0, z_0\}$ specifies the onset of the absorbing potential along each coordinate axis. The parameter η has dimensions of energy per length squared, ensuring that $\eta \hat{W}$ is dimensionally consistent with the Hamiltonian. Throughout this work, η is given in atomic units ($E_h a_0^{-2}$).

It is important to note that while \hat{H} is Hermitian, the introduction of the CAP makes $\hat{H}(\eta)$ a complex symmetric operator, satisfying $\hat{H}(\eta) = \hat{H}(\eta)^T$. As a result, the eigenvalues and eigenvectors become complex, and the left and right eigenvectors are related by simple transposition.

Due to the symmetric but non-Hermitian nature of $\hat{H}(\eta)$, the usual stationary principle must be adapted by replacing the standard complex inner product with the so-called c-product, as introduced by Moiseyev.¹⁵⁸ This leads to the following stationary expression for the complex energy

$$E(\eta) = \langle \Psi | \hat{H}(\eta) | \Psi \rangle_c \quad (5)$$

where the trial wave function Ψ is c-normalized such that $\langle \Psi | \Psi \rangle_c = 1$, and the c-product is defined as

$$\langle fg \rangle_c = \int f(\mathbf{r})g(\mathbf{r}) d\mathbf{r} \quad (6)$$

This definition ensures that the energy functional is stationary at eigenfunctions of $\hat{H}(\eta)$, consistent with its complex symmetric structure. In principle, with a complete basis set, the resonance energy can be obtained by taking the limit $\eta \rightarrow 0^+$. However, in practical calculations with finite basis sets, one must determine an optimal, small but nonzero value of η , denoted η_{opt} . This value balances two competing errors: the perturbation introduced by the CAP (which grows with η) and the incompleteness error of the basis set (which diminishes with η).

Riss and Meyer⁴⁰ proposed that η_{opt} can be identified by minimizing the so-called *energy velocity*

$$\eta_{\text{opt}} = \operatorname{argmin}_{\eta} \left| \eta \frac{dE(\eta)}{d\eta} \right| \quad (7)$$

Practically, this involves plotting the trajectory of $E(\eta)$ as a function of η in the complex plane and locating the minimum of the energy velocity. Analytical continuation using a Padé approximant has also been proposed to bypass this optimization (see, for example, ref 159).

2.2. Complex Hartree–Fock Theory. As a first step, we perform a complex restricted Hartree–Fock (cRHF) calculation incorporating the CAP to obtain a mean-field reference wave function and energy for the (closed-shell) neutral system. Therefore, we add the complex potential to the usual Fock matrix

$$\mathbf{F}(\eta) = \mathbf{F} - i\eta \mathbf{W} \quad (8)$$

where \mathbf{F} is the (complex-valued) Fock matrix in the (real-valued) atomic orbital basis, which contains the one-electron core Hamiltonian, as well as the two-electron Hartree and exchange contributions. The elements of \mathbf{W} are the one-electron CAP contributions in the same basis.

Diagonalizing the η -dependent Fock matrix, $\mathbf{F}(\eta)$, yields complex molecular orbitals and energies, represented by the matrix of right eigenvectors $\mathbf{C}(\eta)$, which are normalized with respect to the c-product, such that

$$\mathbf{C}(\eta)^T \cdot \mathbf{S} \cdot \mathbf{C}(\eta) = \mathbf{I} \quad (9)$$

Here, \mathbf{S} is the overlap of the atomic basis functions. In practice, this step is performed via a modified Cholesky decomposition.¹⁶⁰ The HF equations are iteratively solved until self-consistency is reached. Note that we do not apply any projection to reduce the unphysical perturbation of the occupied orbitals introduced by the CAP.¹⁶¹

2.3. Complex GW Approximation. As a second step, we carry out a complex-valued *GW* calculation which explicitly incorporates the CAP to access the anionic resonances starting from the neutral reference state. In this work, we present the essential equations for understanding and implementing the complex *GW* formalism, and we direct readers interested in further details to several dedicated reviews^{75,76,162–164} and textbooks.^{71–73,165}

Within the four-point formalism,^{111,166–169} the instantaneous Coulomb potential is expressed as

$$v(12; 1'2') = \delta(11') \frac{\delta(t_1 - t_2)}{|\mathbf{r}_1 - \mathbf{r}_2|} \delta(22') \quad (10)$$

where $\delta(11')$ represents the Dirac delta function. The indices, such as 1, denote shorthand notation for both time coordinates (t_1) and the spin-space coordinates $\mathbf{x}_1 = (\sigma_1, \mathbf{r}_1)$ for each particle.

In practical applications of the *GW* approximation, the process begins with a reference propagator G_0 , typically derived from a mean-field model. To keep things simple, we illustrate the coupled integro-differential equations for the *GW* formalism when $G_0 = G_{\text{HF}}$ is used as the reference propagator. Note that, in the present context, the HF orbitals and their corresponding energies are already complex-valued (see Section 2.2).

The total self-energy can be decomposed into three components: the Hartree (H), exchange (x), and correlation (c) contributions, such that

$$\Sigma(11') = \Sigma_H(11') + \Sigma_x(11') + \Sigma_c(11') \quad (11)$$

The exchange–correlation part, denoted $\Sigma_{xc} = \Sigma_x + \Sigma_c$, is calculated as the convolution of the one-body interacting Green's function G with the dynamically screened Coulomb interaction W

$$\Sigma_{xc}(11') = i \int d(22') G(22') W(12'; 21') \quad (12)$$

Here, W is determined via the irreducible polarizability \tilde{L} as follows

$$W(12; 1'2') = v(12^-; 1'2')$$

$$-i \int d(343'4') W(14; 1'4') \tilde{L}(3'4'; 3^+4) v(23; 2'3') \quad (13)$$

A superscript over an index, such as 1^\pm , indicates an infinitesimal time shift, i.e., $t_{1\pm} = t_1 \pm \tau$ ($\tau \rightarrow 0^+$).

The irreducible polarizability \tilde{L} in the *GW* approach is approximated as the product of two Green's functions

$$\tilde{L}(12; 1'2') = G(12') G(21') \quad (14)$$

The Green's function itself is computed via the Dyson equation

$$G(11') = G_{\text{HF}}(11') + \int d(22') G_{\text{HF}}(12) \Sigma_c(22') G(21') \quad (15)$$

To describe quasiparticles, it is often convenient to introduce a set of spin–orbital basis functions $\{\varphi_p\}_{1 \leq p \leq K}$ associated with energies $\{\epsilon_p\}_{1 \leq p \leq K}$. In the absence of a CAP, both quantities are real-valued, reflecting the Hermitian nature of the underlying operators. However, when a CAP is present, the energies and the corresponding orbitals generally become complex.

Within this spin–orbital basis, the Lehmann representation of G is given by

$$G(\mathbf{x}_1, \mathbf{x}_1; \omega) = \sum_i \frac{\varphi_i(\mathbf{x}_1)\varphi_i(\mathbf{x}_1)}{\omega - \epsilon_i - i\kappa} + \sum_a \frac{\varphi_a(\mathbf{x}_1)\varphi_a(\mathbf{x}_1)}{\omega - \epsilon_a + i\kappa} \quad (16)$$

Here, the indices a, b, \dots represent the V virtual orbitals (states above the Fermi level), i, j, \dots denote the O occupied orbitals (states below the Fermi level), and ν labels single (de)-excitation (ia). The indices p, q, \dots are used for arbitrary orbitals, and we have $K = O + V$. The parameter $\kappa > 0$ is a small positive broadening term that ensures the correct causal structure of the Green's function. It is commonly denoted as η in the literature, but we use κ here to avoid confusion with the CAP strength parameter [see eq 2]. Note that, due to the use of the c-product, the orbitals in eq 16 are not complex-conjugated.

By performing Fourier transforms and projecting onto the spin–orbital basis, we can derive the matrix elements for the correlation part of the self-energy

$$\begin{aligned} [\Sigma_c(\omega)]_{pq} &= \sum_{i\nu} \frac{M_{pi,\nu} M_{qi,\nu}}{\omega - \epsilon_i + \Omega_\nu - i\kappa} \\ &+ \sum_{a\nu} \frac{M_{pa,\nu} M_{qa,\nu}}{\omega - \epsilon_a - \Omega_\nu + i\kappa} \end{aligned} \quad (17)$$

The transition densities are expressed as

$$M_{pq,\nu} = \sum_{ia} [\langle p|alqi\rangle_c X_{ia,\nu} + \langle pilqa\rangle_c Y_{ia,\nu}] \quad (18)$$

Here, the bracket notation represents the electron repulsion integrals

$$\langle pqrls\rangle_c = \iint \frac{\varphi_p(\mathbf{x}_1)\varphi_q(\mathbf{x}_2)\varphi_r(\mathbf{x}_1)\varphi_s(\mathbf{x}_2)}{|\mathbf{r}_1 - \mathbf{r}_2|} d\mathbf{x}_1 d\mathbf{x}_2 \quad (19)$$

The excitation energies Ω_ν , satisfying $\text{Re}(\Omega_\nu) > 0$, and the corresponding amplitudes $X_{ia,\nu}$ and $Y_{ia,\nu}$ are obtained by solving a Casida-like¹⁷⁰ RPA^{171–174} eigenproblem in the basis of single excitations ($i \rightarrow a$) and deexcitations ($a \rightarrow i$)

$$\begin{pmatrix} \mathbf{A} & \mathbf{B} \\ -\mathbf{B} & -\mathbf{A} \end{pmatrix} \cdot \begin{pmatrix} \mathbf{X} & \mathbf{Y} \\ \mathbf{Y} & \mathbf{X} \end{pmatrix} = \begin{pmatrix} \mathbf{X} & \mathbf{Y} \\ \mathbf{Y} & \mathbf{X} \end{pmatrix} \cdot \begin{pmatrix} \boldsymbol{\Omega} & \mathbf{0} \\ \mathbf{0} & -\boldsymbol{\Omega} \end{pmatrix} \quad (20)$$

Here, \mathbf{X} and \mathbf{Y} are matrices whose columns are the eigenvectors X_ν and Y_ν , respectively, and $\boldsymbol{\Omega}$ is a diagonal matrix with eigenvalues Ω_ν on the diagonal, representing the excitation energies. The matrix elements of \mathbf{A} and \mathbf{B} are defined as

$$A_{ia,jb} = (\epsilon_a - \epsilon_i)\delta_{ij}\delta_{ab} + \langle ajlib\rangle_c \quad (21a)$$

$$B_{ia,jb} = \langle ablji\rangle_c \quad (21b)$$

Unlike the usually employed complex version of eq 20, which involves complex conjugation of the amplitudes,¹⁷⁵ this

formulation does not, owing to the use of the complex symmetric c-product in place of the standard Hermitian scalar product, such that $\langle ijlab\rangle_c = \langle ablji\rangle_c$.

We impose the following normalization conditions on the solutions \mathbf{X} and \mathbf{Y} similar to the real case¹⁷⁶

$$\mathbf{X}^T \cdot \mathbf{X} - \mathbf{Y}^T \cdot \mathbf{Y} = \mathbf{1} \quad (22a)$$

$$\mathbf{X}^T \cdot \mathbf{Y} - \mathbf{Y}^T \cdot \mathbf{X} = \mathbf{0} \quad (22b)$$

2.4. Self-Consistent GW Schemes. We now shift our attention to the computation of the Dyson orbitals φ_p and quasiparticle energies ϵ_p . The Dyson eq 15 implies that these quantities should satisfy the following dynamical non-Hermitian equation

$$[f + \Sigma_c(\omega = \epsilon_p)]\varphi_p = \epsilon_p \varphi_p \quad (23)$$

where f represents the Fock operator in the molecular orbital basis. However, the frequency dependence of the correlation self-energy Σ_c introduces nonlinearity and complexity to this quasiparticle equation, prompting the use of various approximations.

The G_0W_0 scheme, for instance, involves a single-shot iteration of eq 23 by considering only the diagonal elements of the self-energy.^{140–146} In this approach, starting from one-electron HF orbitals φ_p^{HF} with energies ϵ_p^{HF} , the following equation is solved

$$\epsilon_p^{\text{HF}} + [\Sigma_c(\omega = \epsilon_p)]_{pp} = \epsilon_p \quad (24)$$

By performing a root search using the Newton–Raphson algorithm starting from the mean-field energies, we aim to locate the quasiparticle solutions, i.e., the roots of the nonlinear equations that carry the largest spectral weights

$$Z_p = \frac{1}{1 - \left. \frac{\partial \Sigma_c(\omega)}{\partial \omega} \right|_{\omega=\epsilon_p}} \quad (25)$$

The evGW method, where only the quasiparticle energies are revised, takes a more iterative approach by updating, at each step, the RPA eigenvectors \mathbf{X}_ν and \mathbf{Y}_ν used to construct the transition densities [see eq 18], the RPA neutral excitation energies Ω_ν and quasiparticle energies ϵ_p involved in the expression of the RPA matrix elements [see eqs 21a and 21b] and the self-energy [see eq 17]. This iterative refinement of the self-energy leads to progressively improved quasiparticle energies until convergence is achieved.^{137,147–150}

In the qsGW approach, both orbitals and energies are updated self-consistently until convergence is reached.^{128,151–157} This is accomplished by iteratively diagonalizing an effective Fock-like operator

$$(f + \tilde{\Sigma}_c)\varphi_p = \epsilon_p \varphi_p \quad (26)$$

where the correlation part of the self-energy is approximated by a static, Hermitian operator $\tilde{\Sigma}_c$ with matrix elements given by

$$[\tilde{\Sigma}_c]_{pq} = \frac{[\Sigma_c(\omega = \epsilon_p)]_{pq} + [\Sigma_c(\omega = \epsilon_q)]_{qp}}{2} \quad (27)$$

Note that, thanks to the orbital self-consistency, the qsGW results (or, more generally, the manifold of solutions) are independent of the starting set of orbitals.

It should be noted that the construction in eq 27 corresponds to the so-called “mode A” introduced by Kotani,

van Schilfgaarde, and Faleev.¹⁵⁴ In the same work, the authors proposed an alternative construction, “mode B”, which is often used in qsGW implementations that rely on analytical continuation of the self-energy.^{116,177,178} In mode B, the off-diagonal elements of the self-energy are evaluated at the Fermi energy, which is numerically more stable than evaluating them far from it. This improves convergence while producing results that are essentially comparable to mode A. However, because the expression of eq 27 is more common, we will only consider mode A in the present study.

A recent alternative to the qsGW self-energy, based on a similarity renormalization group (SRG) approach, has been proposed.¹⁵⁷ We extended this method for complex-valued energies. The expressions for the self-energy can be found in Appendix B. The SRG regularizes the self-energy, in contrast to the approach of eq 27. Such regularization is crucial, as achieving convergence in a large basis set, required to treat resonances at the qsGW level, is generally challenging. The SRG-regularized self-energy and the form given in eq 27 are closely related. The former depends on a flow parameter s . In the limit $s \rightarrow \infty$, both yield identical diagonal components of the self-energy, leading to very similar final results. Conversely, at $s = 0$, the method reduces to the mean-field approximation, recovering the corresponding orbital energies and orbitals. The same renormalization can be used for evGW. In the following, unless otherwise stated, we use the renormalized version of the evGW and qsGW methods to improve convergence.

As discussed in Section 1, resonance states are characterized by complex energies with a small negative imaginary component, reflecting their finite lifetimes. To identify such a state, we first perform a calculation on the neutral molecule and then examine the quasiparticle energies ϵ_p with real part above the Fermi level, corresponding to electron attachment processes. Among the states within a given real component energy window, the resonance is identified as the one with the smallest imaginary part, indicating the longest lifetime and the most bound-state-like character. Its position and width are given by

$$E_R = \text{Re}(\epsilon_p) \quad \Gamma = -2\text{Im}(\epsilon_p) \quad (28)$$

in accordance with eq 1. These definitions apply both at the HF and the GW levels of theory. At the HF level, this approximation to IPs and EAAs is commonly referred to as Koopmans’ theorem.¹⁷⁹

As mentioned in Section 1, GW can be implemented with cubic scaling, thanks to numerous innovative algorithmic developments.^{87,92,117–133} In particular, a cubic-scaling implementation of qsGW was recently reported by Förster and Visscher.¹²⁸ As a result, partially self-consistent GW schemes can now be applied to molecular systems beyond the size limit of wave function methods like EOM-CCSD. Nonetheless, it is worth mentioning that our current implementation scales as $O(K^6)$ due to the diagonalization of the RPA eigenproblem (20).

2.5. Spectral Function. The single-particle Green’s function provides direct access to the spectral function

$$A_p(\omega) = \frac{1}{\pi} |\text{Im}G_p(\omega)| \quad (29)$$

of each quasiparticle state p , as well as to the total spectral density

$$A(\omega) = \sum_p A_p(\omega) \quad (30)$$

In G_0W_0 and evGW, where the self-energy is ω -dependent, the spectral function becomes

$$A_p(\omega) = \frac{1}{\pi} \frac{|I(\omega)|}{R(\omega)^2 + I(\omega)^2} \quad (31)$$

with

$$R(\omega) = \text{Re}\{\omega - \epsilon_p^{\text{HF}} - [\Sigma_c(\omega)]_{pp}\} \quad (32a)$$

$$I(\omega) = \text{Im}\{\epsilon_p^{\text{HF}} + [\Sigma_c(\omega)]_{pp} - \text{sgn}[\text{Re}(\epsilon_p^{\text{HF}} - \mu)]\kappa\} \quad (32b)$$

where μ is the chemical potential. For the qsGW with static self-energy, the spectral function is given by

$$A_p(\omega) = \frac{1}{\pi} \frac{|\text{Im}\{\epsilon_p - \text{sgn}[\text{Re}(\epsilon_p - \mu)]\kappa\}|}{\text{Re}(\omega - \epsilon_p)^2 + \text{Im}\{\epsilon_p - \text{sgn}[\text{Re}(\epsilon_p - \mu)]\kappa\}^2} \quad (33)$$

In standard GW calculations, a finite broadening parameter κ is typically introduced to generate a nonzero width, i.e. finite lifetime. In our CAP-based approach, however, an imaginary part to the energies is inherently introduced, effectively regularizing the Green’s function and eliminating the need for artificial broadening.

3. COMPUTATIONAL DETAILS

The various flavours of CAP-GW developed here have been implemented in an open-source in-house program, named QUACK.¹⁸⁰ The one-electron CAP integrals have been computed with OPENCAP 1.2.7.¹⁸¹ For the six small molecules investigated here, the CAP onsets, as well as the bond lengths and the bond angles, are given in Table 1. In addition, we

Table 1. Parameters Employed for the CAP Calculations: CAP Onset (x_0, y_0, z_0), Bond Lengths and Angles^a

system	(x_0, y_0, z_0)	bond length	bond angle
N_2^-	(2.76, 2.76, 4.88)	$R_{\text{NN}} = 2.0740$	
CO^-	(2.76, 2.76, 4.97)	$R_{\text{CO}} = 2.1316$	
C_2H_2	(3.20, 3.20, 6.35)	$R_{\text{CC}} = 2.2733$	$\angle_{\text{CH}} = 180.0$
		$R_{\text{CH}} = 2.0088$	
C_2H_4^-	(7.1, 4.65, 3.40)	$R_{\text{CC}} = 2.5303$	$\angle_{\text{CH}} = 121.2$
		$R_{\text{CH}} = 2.0522$	
CH_2O^-	(3.85, 2.95, 6.10)	$R_{\text{CO}} = 2.2771$	$\angle_{\text{HCO}} = 121.9$
		$R_{\text{CH}} = 2.0995$	
CO_2^-	(3.33, 3.33, 9.57)	$R_{\text{CO}} = 2.1978$	
		$R_{\text{CH}} = 2.0995$	

^aAll lengths are in bohr and all angles in degrees. The molecular orientation with respect to the CAP can be seen in the Supporting Information.

provide, in the Supporting Information, the geometry files and basis sets. For the SRG, we systematically used $s = 500$, unless otherwise stated. This ensures good convergence to the result obtained without regularization.¹⁵⁷ Additionally, to improve the convergence of the self-consistent HF and qsGW procedures, we rely on Pulay’s DIIS algorithm,^{182,183} here adapted for complex algebra with the c-product. The exact implementation of this adaptation is outlined in Appendix A. The qsGW calculations are carried out with a convergence

threshold of 5×10^{-4} a.u. on the usual commutator norm.¹⁸⁴ Under these conditions, such calculations typically converge within approximately four or five iterations. We calculate the derivatives needed to obtain the energy velocity [see eq 7] by the standard second-order finite difference scheme using a step size of 5×10^{-5} for η .

The broadening parameter κ is set to zero in all CAP-GW calculations. Both the GW approximation and the CAP formalism are always applied to all occupied and virtual orbitals. For G_0W_0 and evGW, quasiparticle energies are computed by directly solving the nonlinear, frequency-dependent quasiparticle equation, without resorting to linearization. Our study is limited to closed-shell neutral reference systems, consistently employing a restricted formalism. Throughout this work, HF orbitals and energies are systematically used as the starting point, a choice justified by the relatively small size of the molecular systems considered.

For all calculations in this work, we employ the aug-cc-pVTZ + 3s3p3d basis set. This corresponds to the standard aug-cc-pVTZ basis set, augmented by three additional diffuse functions of each angular momentum type (s, p, and d), centered at the geometric center of the molecule. For each angular momentum, the exponent of the first added diffuse function is chosen as half the average of the smallest exponents of the functions centered at the unique non-hydrogen atoms. The remaining two exponents for each angular momentum are generated by successively halving the previous one, forming a geometric progression. The same basis set has been employed in several previous studies.^{43,53,185} Full details of the basis sets used in this study are provided in the Supporting Information.

4. RESULTS

4.1. N₂⁻. **4.1.1. Context and Approach.** The N₂⁻ temporary anion, corresponding to a $^2\Pi_g$ configuration, is one of the most extensively studied resonances. It therefore serves as the first benchmark system for our method and is discussed in greater detail to provide the necessary context for interpreting the results of systems examined subsequently. For each system and method, we provide Dyson orbitals that confirm the electronic configuration, as well as energy-velocity plots, in the Supporting Information.

We begin with a brief overview of results obtained using various related theoretical approaches. While not intended to be comprehensive, this overview serves to place our findings in the appropriate context. We then present the results obtained with the methods introduced in this work.

Starting at the lowest level of theory, we present a more qualitative discussion, as these results are inherently less accurate by design. As described in Section 2.2, we implemented a complex restricted HF method incorporating a CAP. Koopmans' theorem provides a mean-field estimate of the EA. This level of theory is highly approximate, even more so than other mean-field approaches that perform self-consistent calculations for both the neutral and anionic species. The energy difference in the latter yields the EA while accounting for state-specific orbital relaxation, commonly known as the ΔSCF method.

ΔSCF calculations targeting the resonance require a state-specific HF formulation, which is feasible but beyond the scope of this work. Comparing our Koopmans-level results with literature ΔSCF data,⁶² both methods overestimate the resonance position by roughly 1 eV, while we overestimate the width by a factor of about two. In contrast, ΔSCF yields

more reasonable widths. Nevertheless, our method successfully identifies the resonance and provides rough estimates of the position and width. Thus, it serves as a suitable mean-field starting point for subsequent GW corrections, rather than final predictive results.

At a comparable level of correlation treatment, GW methods have been combined with the stabilization technique, which estimates the position and width by analytic continuation.⁷⁷ In that study, G_0W_0 underestimates the width obtained by EOM-CCSD with analytic continuation by more than a factor of 4. In contrast, a self-consistent GW approach that includes orbital relaxation yields lifetimes of the correct order of magnitude.⁷⁷

Furthermore, Green's function methods combined with CAP have been applied in previous studies using different basis sets than those employed in our work, making a direct comparison difficult. Nevertheless, these approaches have been shown to yield reasonable estimates for both the resonance position and width. For instance, reported values including basis set uncertainty are 2.58(13) eV for the position and 0.55(14) eV for the width.⁶⁵ Despite the methodological and basis set differences, our qsGW results for the resonance position largely fall within the reported error margins (see Table 2). However, the resonance width at the second minimum (see below) deviates by 0.17 eV.

Table 2. Optimal CAP Strengths, Resonance Positions, and Widths of N₂⁻ Obtained Using Different Methods^d

method	η_{opt} (a.u.)	E_R (eV)	Γ (eV)
G_0W_0	0.00170*	2.977	0.484
G_0W_0	0.01150	2.765	0.244
evGW	0.00170*	2.963	0.446
evGW	0.01325	2.725	0.240
qsGW	0.00160	2.565	0.460
qsGW	0.00780	2.707	0.386
CAP-EOM-EA-CCSD ⁴³	0.0015	2.487	0.417
CAP-exFCI ⁵³	0.0015*	2.449	0.391
CAP-EOM-EA-CCSD ⁶³	0.0070	2.617	0.395
CAP-EOM-EA-CCSD ^{188a}	0.0020	2.461	0.428
CAP-EOM-EA-CCSD ^{187b}	0.0022	2.511	0.407
experiment ^{189c}		2.316	0.414

^aValues obtained using the aug-cc-pVQZ basis set augmented by three sets of s-, p-, and d-type diffuse functions on each atom. ^bValues obtained using the aug-cc-pVTZ basis set augmented by six sets of s-, p-, and d-type diffuse functions on each atom. ^cValues obtained by fitting a theoretical model to experimental data. ^dThe GW results are from this work; other data are taken from the cited references. Optimal η values marked with * are derived by another method as described in the main text.

We now turn to the highest level of theory combined with a CAP: extrapolated full configuration interaction (exFCI), which treats all electronic correlations.⁵³ Due to its high computational cost, reference data are limited. For N₂⁻ and CO⁻, however, exFCI results⁵³ are available at the optimal CAP strength η obtained from EOM-EA-CCSD calculations.⁴³ Comparing EOM-EA-CCSD to exFCI reveals smaller deviations than those observed between our GW results and EOM-EA-CCSD. We remark that the deviations are in the expected order of magnitude of CCSD to FCI for neutral excitations (see Table 2).¹⁸⁶ Since exFCI data is available only for selected systems and lacks η -optimization, while EOM-EA-CCSD

values exist for all systems studied in this work, we adopt CAP-EOM-EA-CCSD as our primary theoretical reference.

For N_2^- , resonance positions and widths derived by CAP-EOM-EA-CCSD have been reported at significantly different CAP strengths: One at $\eta = 0.0015$ ⁴³ and one at $\eta = 0.007$.⁶³ Those values correspond to two different local minima in the energy velocity. We observe a qualitatively similar behavior and trajectory using the qsGW method (see Figure 1). Similar

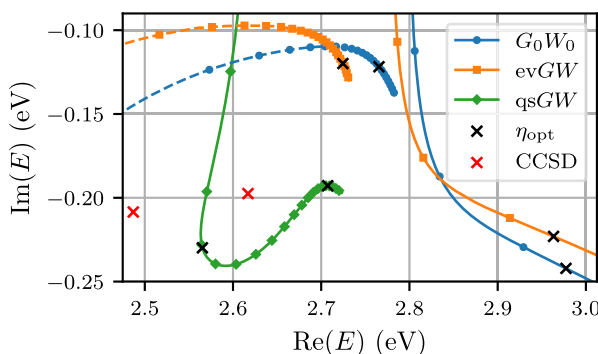


Figure 1. Trajectories of N_2^- computed at different levels of self-consistency. For G_0W_0 and $\text{ev}GW$, the solid line denotes the trajectory associated with the first energy-velocity minimum, while the dashed line corresponds to the second minimum. Black crosses indicate the positions of the energy-velocity minima, representing the final results for the resonance state. Red crosses show the CAP-EOM-EA-CCSD reference values (see Table 2). The maximum η value shown is 0.0155 for G_0W_0 and $\text{ev}GW$, and 0.01 for $\text{qs}GW$.

multiple-minimum structures also appear in other systems studied. This phenomenon may arise from the limited size of the basis set.^{187,188} Here, our goal is to assess the performance of CAP-GW approaches relative to higher-level theories. Whenever available, we also include results obtained with larger basis sets. For N_2^- , we analyze both reported minima. For the remaining systems, multiple minima are mentioned when encountered, but we report only the results that correspond to the CAP-EOM-EA-CCSD reference. Furthermore, we note that all CAP-EOM-EA-CCSD values reported in the following tables and figures correspond to unprojected, thus “full”, CAP calculations.

4.1.2. Trajectories, Positions and Lifetimes. Within the qsGW framework, a single state can be followed continuously along the η -trajectory to identify both minima. In contrast, for methods based on HF orbitals, such as G_0W_0 and $\text{ev}GW$, two distinct trajectories must be tracked (see Figure 1). These apparently describe the same resonance state, but at different values of η . Moreover, for these HF-based methods, no local minimum is found in the vicinity of the first reported minimum, except at the Koopmans level of theory, at $\eta = 0.0017$. We therefore adopt this value to estimate the resonance parameters in G_0W_0 and $\text{ev}GW$.

Also, in $\text{ev}GW$, the η -trajectory was not smooth enough to reliably identify the second reported minimum of the energy velocity using finite differences. We thus performed additional calculations with $s = 100$ to identify the optimal η value.

Our results are presented in Table 2. We find that all discussed GW methods overestimate the resonance position compared to reference theoretical methods and experiment. While the G_0W_0 and $\text{ev}GW$ methods deviate by approximately 0.5 eV from the CAP-EOM-EA-CCSD reference for the first minimum, they are only off by about 0.1 eV for the second

minimum. On the other hand, these methods yield a more accurate lifetime for the first minimum than for the second. The $\text{qs}GW$ method, by contrast, closely reproduces the reference values, with differences of about 0.1 eV for the resonance position and 0.05 eV for the width Γ . Compared to experimental data, all GW methods, as well as the CAP-EOM-EA-CCSD approach, systematically overestimate the resonance position. Furthermore, $\text{ev}GW$ and G_0W_0 underestimate the resonance width by more than 0.17 eV compared to both theoretical and experimental values.

These observations strongly suggest that orbital relaxation effects, accounted for only in the $\text{qs}GW$ method, are essential not only for reliably determining η_{opt} but also for accurately describing the underlying resonance state.

4.1.3. Spectral Function. Figure 2 compares spectral functions obtained from the $\text{qs}GW$ method with and without

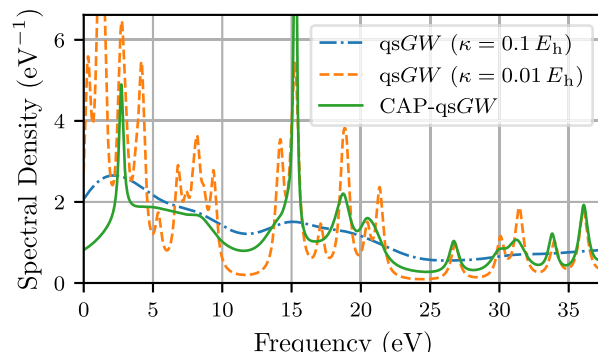


Figure 2. Comparison of the spectral function of N_2 derived by CAP-augmented $\text{qs}GW$ (CAP- $\text{qs}GW$) with $\eta_{\text{opt}} = 0.0078$ (green curve) and $\text{qs}GW$ without CAP but with broadening parameter $\kappa = 0.1 E_h$ (blue curve) and $\kappa = 0.01 E_h$ (orange curve).

the inclusion of a CAP. We focus here on the CAP-augmented $\text{qs}GW$ (CAP- $\text{qs}GW$) result evaluated at the optimal CAP strength, $\eta_{\text{opt}} = 0.0078$, which corresponds to the lower of the two energy velocity minima discussed earlier. For comparison, we also include spectra computed using fixed artificial broadening parameters, $\kappa = 0.1 E_h$ and $\kappa = 0.01 E_h$.

While these spectral functions offer valuable qualitative insights, their physical interpretation is limited. First, the chosen Gaussian basis set is clearly too small to accurately describe the continuum, whose states are asymptotically plane-wave-like. As the basis set is enlarged by adding more diffuse functions, one would expect an increasingly dense set of discrete states approximating the continuum over a broad energy range. Second, the inclusion of the CAP discretizes the continuum by turning it into a set of complex-valued eigenvalues, with the goal of isolating resonance features. However, the CAP strength η was optimized only for a specific resonance state, so the resulting spectrum captures primarily this state and not the entire unbound spectrum.

In the absence of a CAP, the broadening parameter κ uniformly widens all peaks in the spectral function, regardless of their real part E_R . As a result, increasing κ leads to overly broad and overlapping peaks, obscuring the identification of individual resonances. Reducing κ sharpens the peaks. There is no interpretation of the peak width since κ is an artificial parameter and not physically meaningful. All peaks are broadened with the same κ .

In contrast, the CAP-*qsGW* approach yields a spectral function where each resonance is broadened according to its actual lifetime. The CAP introduces an energy-dependent, non-Hermitian perturbation that allows for a physically meaningful extraction of both the position E_R and the resonance width Γ . Importantly, the full width at half-maximum of a given peak directly corresponds to Γ , the inverse lifetime of the resonance state. Hence, the inclusion of the CAP enables an identification of the metastable state and provides access to its intrinsic lifetime, a quantity inaccessible through the use of a constant broadening parameter alone.

Furthermore, it can be observed that the inclusion of the CAP leads to only a slight shift in the peak positions compared to the artificially broadened spectra. This is particularly evident for the resonance state for which the CAP strength was optimized: the first peak in the CAP-*qsGW* spectral function. Its energy remains nearly unchanged, indicating that the CAP does not significantly alter the resonance position, but rather unveils its physical width in a controlled and interpretable manner.

4.2. CO⁻. The resonance state of CO⁻ is a $^2\Pi$ shape resonance. The trajectories obtained from the different *GW* methods are shown in Figure 3. In contrast to N₂⁻, clear

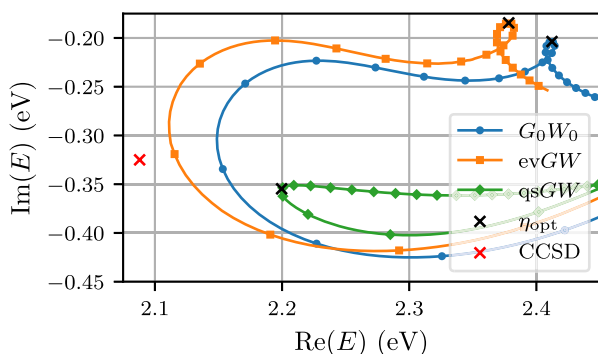


Figure 3. Trajectories of CO⁻ computed at different levels of self-consistency. Black crosses indicate the positions of the energy-velocity minima, representing the final results for the resonance state. Red crosses show the CAP-EOM-EA-CCSD reference values (see Table 3). The maximal η value shown is 0.014 for all methods.

minima in the energy velocity are identifiable at all three levels of self-consistency, as well as at the Koopmans level. However, the trajectories of evGW and G_0W_0 differ markedly in shape from that of qsGW, and their minima appear at different locations along the trajectories. As a result, the optimal CAP strengths η_{opt} for evGW and G_0W_0 are more than twice as large as that of qsGW.

The evGW and G_0W_0 trajectories exhibit broad turns followed by loops in the upper right corner of the frame, corresponding to the velocity minima. In contrast, the qsGW trajectory features a much sharper turn, closely resembling the shape obtained from CAP-EOM-EA-CCSD.⁶³ This qualitative agreement suggests that orbital relaxation plays a significant role in accurately describing the resonance state of CO⁻, and that qsGW, through its self-consistency in both eigenvalues and orbitals, is better suited to capture orbital relaxation. We also find another local minimum of the energy velocity at the qsGW level for $\eta = 0.0006$, which is less pronounced and yields a higher energy velocity than the one previously reported. Therefore, we assume it arises from the limitations of the finite basis set.

The numerical resonance parameters are summarized in Table 3. As shown there, G_0W_0 and evGW yield very similar

Table 3. Optimal CAP Strengths, Resonance Positions, and Widths of CO⁻ Obtained Using Different Methods^c

method	η_{opt} (a.u.)	E_R (eV)	Γ (eV)
G_0W_0	0.00870	2.412	0.407
evGW	0.00875	2.378	0.369
qsGW	0.00295	2.200	0.709
CAP-EOM-EA-CCSD ⁴³	0.0028	2.088	0.650
CAP-EOM-EA-CCSD ^{188a}	0.0018	2.010	0.775
CAP-EOM-EA-CCSD ^{187b}	0.0054	2.02	0.64
CAP-exFCI ⁵³	0.0028*	2.060	0.611
experiment ^{190–192}		1.9–2.0	
		1.93 ¹⁹²	0.75 ¹⁹²
			0.80(3) ¹⁹¹

^aValues obtained using the aug-cc-pVQZ basis set augmented by three sets of s-, p-, d- and f-type diffuse functions on each atom.

^bFirst-order corrected energies using the aug-cc-pVTZ basis set augmented by six sets of s-, p-, and d-type diffuse functions on each atom. ^cThe GW results are from this work; other data are taken from the cited references. The optimal η value marked with * is derived by another method as described in the main text.

results, differing by only about 0.04 eV in both the resonance position and width. Both methods, however, underestimate the width predicted by CAP-FCI and CAP-EOM-EA-CCSD by more than 0.2 eV, and deviate even more from experimental data. Additionally, they overestimate the resonance position by more than 0.25 eV compared to the theoretical references. In contrast, qsGW overestimates the theoretical reference position by less than 0.15 eV and width Γ by less than 0.1 eV, representing a noticeable improvement.

We compare our results to estimates of the *vertical* resonance position, that is, at the bond length of the neutral molecule, and not the adiabatic value of 1.50 eV reported in refs 190–192. From the parameters provided in these works, we estimated an experimental vertical resonance position of 1.93 eV, which aligns well with the cross section maximum of more recent experiments, peaking between 1.9 and 2.0 eV.^{193–195} Thus, both CAP-EOM-EA-CCSD and CAP-exFCI slightly overestimate the resonance position relative to experiment. The discrepancy between qsGW and experiment is also moderate, on the order of 0.3 eV. Furthermore, for the imaginary part of the energy, qsGW provides better agreement with experimental data than the other theoretical methods.

4.3. C₂H₂⁻. The resonance state of C₂H₂⁻ is a $^2\Pi_g$ shape resonance. The CAP trajectories obtained from the three *GW* methods are shown in Figure 4. In contrast to the case of CO⁻, all methods— G_0W_0 , evGW, and qsGW—yield qualitatively similar trajectories, characterized by smoothly curved paths with clearly defined minima in the energy velocity. This similarity in shape indicates that the underlying electronic structure and its response to the CAP are treated consistently across all levels of self-consistency. Even though we find only one minimum for each method, the slope of the energy velocity decreases and then increases again around $\eta = 0.001$. This behavior is consistent with the pattern observed for the other molecules, where shallow local minima appear at small values of η .

The minor variations in the shape of the trajectories are reflected in the extracted resonance parameters (see Table 4).

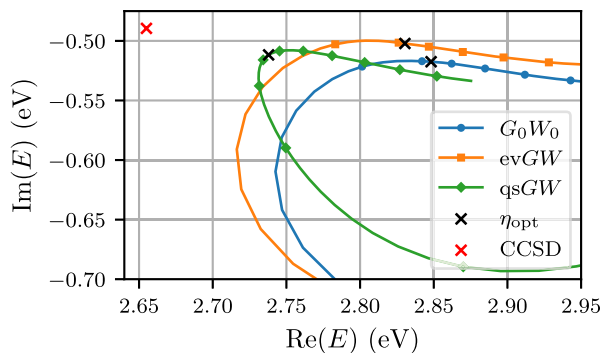


Figure 4. Trajectories of C_2H_2^- computed at different levels of self-consistency. Black crosses indicate the positions of the energy-velocity minima, representing the final results for the resonance state. Red crosses show the CAP-EOM-EA-CCSD reference values (see Table 4). The maximal η value shown is 0.007 for all methods.

Table 4. Optimal CAP Strengths, Resonance Positions, and Widths of C_2H_2^- Obtained Using Different Methods^a

method	η_{opt} (a.u.)	E_{R} (eV)	Γ (eV)
G_0W_0	0.00370	2.848	1.035
evGW	0.00365	2.830	1.004
qsGW	0.00375	2.738	1.023
CAP-EOM-EA-CCSD ⁴³	0.0036	2.655	0.979
experiment ^{196–200}		2.5–2.6	

^aThe GW results are from this work; other data are taken from the cited references.

The optimal CAP strengths η_{opt} are nearly identical across methods, and the resonance positions differ by less than 0.12 eV. The computed widths Γ are also closely aligned, with a spread of only 0.03 eV among the methods.

All three GW variants overestimate the resonance position relative to the CAP-EOM-EA-CCSD reference (2.655 eV), with qsGW performing best among them at 2.738 eV. In terms of resonance width, all GW methods predict it slightly above the CAP-EOM-EA-CCSD value of 0.979 eV, yet within deviations of 0.05 eV. Notably, the best agreement for both position and width is again achieved with qsGW, reinforcing its overall robustness.

In summary, for the $^2\Pi_g$ resonance of C_2H_2^- , all GW methods yield consistent results, both qualitatively and quantitatively. The reduced sensitivity to the level of self-consistency indicates that this system is less impacted by orbital relaxation effects than the systems discussed before.

4.4. C_2H_4^- . The resonance state of C_2H_4^- corresponds to a $^2B_{2g}$ shape resonance. The CAP trajectories obtained from the three GW variants are shown in Figure 5. As in the case of CO^- , the G_0W_0 and evGW trajectories exhibit qualitatively similar behavior, featuring broad turns with identifiable minima in the energy velocity located in the upper-right region of the portrayed frame. However, the trajectory produced by qsGW is markedly different in both shape and curvature, showing no apparent similarity to those of G_0W_0 and evGW.

Despite these differences in trajectory morphology, all three methods yield well-defined minima in the energy velocity. Notably, the optimal CAP strengths η_{opt} differ substantially: G_0W_0 and evGW require relatively large values of η (0.01215 and 0.01055, respectively), while qsGW yields a minimum at a significantly smaller value (0.00475). This again reflects how the interaction with the CAP is handled differently at different

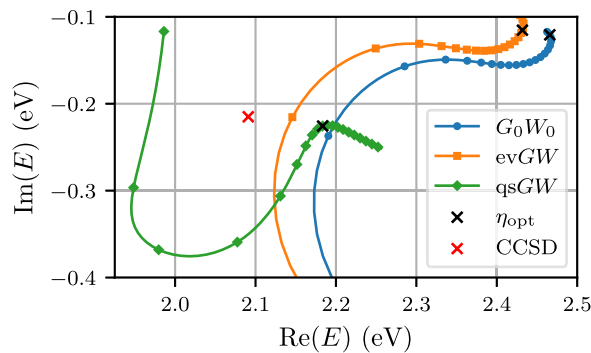


Figure 5. Trajectories of C_2H_4^- computed at different levels of self-consistency. Black crosses indicate the positions of the energy-velocity minima, representing the final results for the resonance state. Red crosses show the CAP-EOM-EA-CCSD reference values (see Table 5). The maximal η value shown is 0.013 for G_0W_0 , 0.014 for evGW and 0.01 for qsGW.

levels of self-consistency, with qsGW requiring a weaker perturbation to stabilize the resonance state. Again, we find another local minimum on the qsGW level at lower $\eta = 0.00095$.

The numerical resonance parameters are summarized in Table 5. The G_0W_0 and evGW variants yield closely aligned

Table 5. Optimal CAP Strengths, Resonance Positions, and Widths of C_2H_4^- Obtained Using Different Methods^b

method	η_{opt} (a.u.)	E_{R} (eV)	Γ (eV)
G_0W_0	0.01215	2.466	0.241
evGW	0.01055	2.432	0.231
qsGW	0.00475	2.183	0.451
CAP-EOM-EA-CCSD ⁴³	0.0046	2.091	0.430
CAP-EOM-EA-CCSD ^{201a}	0.0023	2.028	0.550
experiment ^{202–208}	1.7–1.9	$\leq 0.70^{202}$	

^aValues obtained using the aug-cc-pVTZ basis set augmented by three sets of *s*- and *p*-type diffuse functions on each non-hydrogen atom.

^bThe GW results are from this work; other data are taken from the cited references.

results: they differ by only 0.034 eV in the resonance position and 0.01 eV in the width. However, they significantly overestimate the resonance energy and underestimate the width when compared to the high-level CAP-EOM-EA-CCSD calculation.

In contrast, qsGW produces a resonance energy of 2.183 eV and a width of 0.451 eV, in excellent agreement with the CAP-EOM-EA-CCSD reference values of 2.091 and 0.430 eV, respectively. All theoretical approaches overestimate the resonance position relative to experiment, likely due to limitations in the basis set and the intrinsic challenges of modeling metastable anions.

4.5. CH_2O^- . The resonance state of CH_2O^- corresponds to a 2B_1 shape resonance. The CAP trajectories obtained from the different GW variants are shown in Figure 6. Similar to the case of C_2H_4^- , the trajectories of G_0W_0 and evGW exhibit comparable shapes, both featuring smooth curves with well-defined minima in the energy velocity. In contrast, the qsGW trajectory differs markedly in both geometry and curvature, reflecting the differences in orbital relaxation and self-consistency.

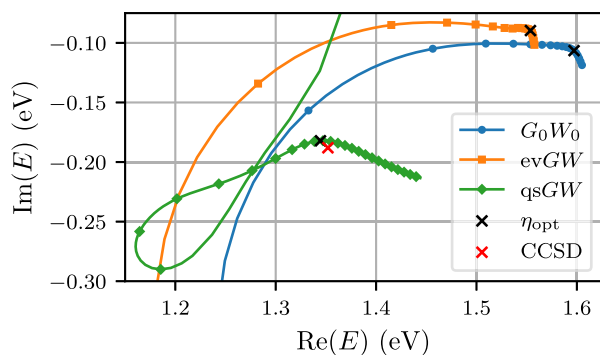


Figure 6. Trajectories of CH_2O^- computed at different levels of self-consistency. Black crosses indicate the positions of the energy-velocity minima, representing the final results for the resonance state. Red crosses show the CAP-EOM-EA-CCSD reference values (see Table 6). The maximal η value shown is 0.012 for all methods.

Despite the differences in trajectory shape, all three methods yield identifiable minima in the energy velocity, allowing for the determination of an optimal CAP strength η_{opt} . The values of η_{opt} for G_0W_0 and $\text{ev}GW$ are nearly identical (0.00915 and 0.00900, respectively), while $\text{qs}GW$ again requires a substantially smaller value (0.00450). This consistent trend across all systems studied suggests that fully self-consistent GW methods ($\text{qs}GW$) can stabilize resonances with weaker perturbations, owing to their more accurate treatment of orbital response in the presence of the CAP. For this molecule, we find an additional local minimum at all levels of self-consistency: at $\eta = 0.000\ 65$ for $\text{qs}GW$, and at $\eta = 0.0013$ for the other two methods.

The corresponding resonance parameters are summarized in Table 6. As in previous systems, G_0W_0 and $\text{ev}GW$ produce

Table 6. Optimal CAP Strengths, Resonance Positions, and Widths of CH_2O^- Obtained Using Different Methods^b

method	η_{opt} (a.u.)	E_R (eV)	Γ (eV)
G_0W_0	0.00915	1.597	0.213
$\text{ev}GW$	0.00900	1.554	0.179
$\text{qs}GW$	0.00450	1.345	0.364
CAP-EOM-EA-CCSD ⁴³	0.0100	1.352	0.376
CAP-EOM-EA-CCSD ^{201a}	0.0018	1.206	0.387
experiment ^{209–211}		0.86–0.87	

^aValues obtained using the aug-cc-pVTZ basis set augmented by three sets of *s*- and *p*-type diffuse functions on each non-hydrogen atom.

^bThe GW results are from this work; other data are taken from the cited references.

similar results, predicting a resonance energy of 1.597 and 1.554 eV, respectively, and widths of 0.213 and 0.179 eV. However, these methods underestimate the resonance width compared to both high-level theory and experiment.

The $\text{qs}GW$ method yields a lower resonance position of 1.345 eV and a broader width of 0.364 eV, in excellent agreement with the CAP-EOM-EA-CCSD values of 1.352 and 0.376 eV, respectively. Although all GW methods overestimate the experimental resonance position, the deviation is significantly smaller for $\text{qs}GW$, suggesting a more realistic description of the resonance state. To the best of our knowledge, no experimental estimate for the resonance width of this system is available.

4.6. CO_2^- . The resonance state of CO_2^- corresponds to a $^2\Pi_u$ shape resonance. The trajectories obtained from various GW methods are shown in Figure 7. In contrast to CO^- , the shape

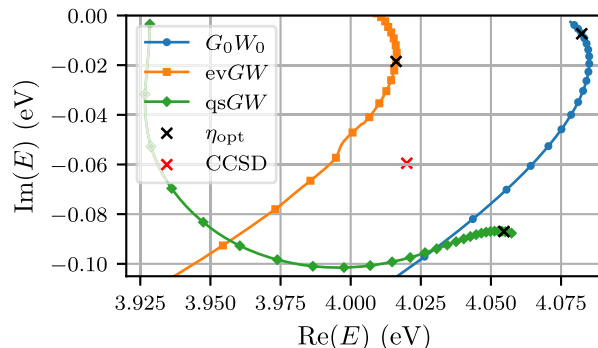


Figure 7. Trajectories of CO_2^- computed at different levels of self-consistency. Black crosses indicate the positions of the energy-velocity minima, representing the final results for the resonance state. Red crosses show the CAP-EOM-EA-CCSD reference values (see Table 7). The maximal η value shown is 0.014 for G_0W_0 , 0.0133 for $\text{ev}GW$ and 0.014 for $\text{qs}GW$.

and behavior of the trajectories differ markedly across methods. While clear local minima in the energy velocity are observed for $\text{qs}GW$ and G_0W_0 , the $\text{ev}GW$ trajectory appears significantly less structured within the examined range. To address this, we performed additional calculations with $s = 100$ to determine an optimal value of η for $\text{ev}GW$. Subsequently, a calculation with $s = 500$ was carried out using this optimal value.

Another related issue with $\text{ev}GW$ is that its self-consistent procedure can converge to different nearby solutions. As a result, varying η does not always lead to the same corresponding GW solution.^{184,212,213} We hypothesize that this is the cause of the small bump observed in the trajectory at $\text{Re}(E) \approx 4.0$ eV. This hypothesis is supported by the fact that no such feature appears in the G_0W_0 calculation. The bump corresponds to a local minimum in the energy velocity, which we disregard due to its likely artificial origin.

In addition, as shown in the trajectory plot (see Figure 7), the imaginary part of the $\text{ev}GW$ energy becomes positive at a certain point. This behavior is unphysical, so we restrict our search for minima to regions of the trajectory where the imaginary part remains negative.

As observed in other molecules, the $\text{qs}GW$ trajectory features a sharp turn that leads to a well-defined minimum, located at a significantly smaller CAP strength, $\eta_{\text{opt}} = 0.000\ 65$, compared to those of G_0W_0 (and $\text{ev}GW$), both of which exhibit broader trajectories and minima at $\eta_{\text{opt}} = 0.012\ 50$ (and 0.009 60). This qualitative behavior again highlights the stabilizing influence of quasiparticle self-consistency in $\text{qs}GW$ and the importance of orbital relaxation for describing resonances.

The resonance parameters are collected in Table 7. At the $\text{qs}GW$ level, the resonance position is $E_R = 4.055$ eV with a width of $\Gamma = 0.174$ eV, showing much closer agreement with CAP-EOM-EA-CCSD and experimental values than the other GW variants. Both the G_0W_0 and $\text{ev}GW$ methods predict higher resonance positions: $E_R = 4.082$ eV for G_0W_0 , and $E_R = 4.016$ eV for $\text{ev}GW$. However, they significantly underestimate the resonance width: $\Gamma = 0.037$ eV for $\text{ev}GW$, and $\Gamma = 0.015$ eV for G_0W_0 .

Table 7. Optimal CAP Strengths, Resonance Positions, and Widths of CO₂⁻ Obtained Using Different Methods^a

method	η_{opt} (a.u.)	E_R (eV)	Γ (eV)
G_0W_0	0.01250	4.082	0.015
evGW	0.00960	4.016	0.037
qsGW	0.01235	4.055	0.174
CAP-EOM-EA-CCSD ⁴³	0.0074	4.020	0.119
experiment ^{202,214–217}		3.6–3.8	0.20 ± 0.07 ²¹⁴

^aThe GW results are from this work; other data are taken from the cited references.

qsGW thus provides a much more realistic description of the metastable state in CO₂⁻, both in terms of position and lifetime. While it still slightly overestimates the resonance position compared to the experimental value (between 3.6 and 3.8 eV), just as CAP-EOM-EA-CCSD, it reproduces the width within the experimental uncertainty (0.20(7) eV),²¹⁴ underlining its strength in treating resonance states where both electron correlation and orbital relaxation are essential.

5. CONCLUSION

We have presented an implementation of the CAP formalism within the GW approximation, enabling the computation of metastable electronic resonance states in a Green's function framework. Applied to a series of prototypical temporary anions of small systems, this approach yields both resonance positions and lifetimes through a fully complex, non-Hermitian treatment.

Among the GW variants considered, the qsGW scheme offers the most reliable performance. Across all studied molecules, qsGW reproduces CAP-EOM-EA-CCSD resonance positions within 0.11 eV and widths within 0.06 eV. The mean absolute differences are only 0.07 eV for the position and 0.03 eV for the width. qsGW systematically overestimates the resonance position relative to CAP-EOM-EA-CCSD, except for CH₂O, where it slightly underestimates it by only 0.007 eV. No clear trend emerges for the widths.

In contrast, G_0W_0 and evGW consistently underestimate resonance widths and predict larger optimal CAP strengths, indicating stronger perturbative effects. These methods also struggle to resolve shallow or less pronounced minima in the CAP energy trajectories, limiting their robustness. Notably, evGW, which includes eigenvalue self-consistency, offers a modest improvement in resonance positions compared to G_0W_0 , but this trend does not extend to the lifetimes.

These findings highlight the importance of orbital relaxation, which is fully accounted for only in qsGW. The close agreement of qsGW with wave function benchmarks suggests that a self-consistent treatment of both eigenvalues and orbitals is critical for a robust description of metastable states. Although all theoretical methods, including CAP-EOM-EA-CCSD, tend to overestimate experimental resonance positions, qsGW provides accuracy on par with high-level wave function theory, delivering reliable estimates for both positions and lifetimes. Thus, qsGW offers a promising and comparatively cheap alternative for describing resonances in larger molecules, where wave function-based methods would be too expensive.

This work opens several avenues for further development. Incorporating first-order perturbative corrections to the CAP energy may enhance reliability, as demonstrated in wave function-based approaches.⁴³ For G_0W_0 and evGW, exploring alternative starting points, such as Kohn–Sham orbitals,²¹⁸

could help mitigate current shortcomings. Furthermore, it would be worthwhile to investigate various flavors of the closely related GF2 (or second Born) methods,^{179,219–236} which circumvent solving the RPA eigenvalue problem by employing an excitation energy and amplitude ansatz based on quasiparticle energies and orbitals. Given their structural similarity to the CAP-GW approach introduced in this work, extending these methods with a CAP should be straightforward. This would also be closely related to the CAP-ADC methods discussed in the introduction.^{64–66,84}

Finally, the methodology presented here could be extended to other metastable phenomena, such as core-ionization and Auger-Meitner decay, where accurate lifetimes are particularly important. In its standard version, the GW formalism is likely not suited for describing Feshbach resonances, which involve two-particle processes, as it is well-known that GW struggles to accurately capture satellite transitions.^{85,237} Nevertheless, a spin-flip extension of GW could in principle be devised to model Feshbach resonances successfully, in analogy with the Bethe–Salpeter equation formalism where such an approach has been applied to access double excitations.²³⁸

It is also worth mentioning that fully self-consistent GW (scGW) methods provide an appealing perspective in the context of resonances.^{113,178,234,235,239,240} In scGW, both orbital energies and eigenfunctions acquire a complex character, and the Green's function naturally incorporates the imaginary broadening that, in G_0W_0 , is usually mimicked by the parameter κ . This feature indeed parallels the role of a CAP. Moreover, since scGW explicitly accounts for orbital relaxation, it may constitute a promising framework for the description of resonances.

APPENDIX A

DIIS

For both the complex self-consistent HF and qsGW methods, we employ the same DIIS protocol. The only difference between the two is the effective Fock operator: for HF, this is the CAP-augmented usual Fock operator in the atomic orbital (AO) basis, $F(\eta)$, while for qsGW it additionally includes the self-energy in the AO basis, $F(\eta) + \Sigma_c$. For simplicity, we omit the explicit η dependence in what follows.

At iteration m , we define the error vector $\mathbf{e}^{(m)}$ as the commutator of the current quantities

$$\mathbf{e}^{(m)} = \mathbf{F} \cdot \mathbf{P} \cdot \mathbf{S} - \mathbf{S} \cdot \mathbf{P} \cdot \mathbf{F} \quad (\text{A1})$$

where \mathbf{P} is the one-electron density matrix in the AO basis, which in the restricted formalism is given by

$$P_{\mu\nu} = 2 \sum_i C_{\mu i} C_{\nu i} \quad (\text{A2})$$

With these ingredients, the DIIS procedure can be applied to accelerate convergence. DIIS minimizes the error by forming a linear combination of n previous error vectors. We first construct the auxiliary matrix

$$E_{k,l} = (\mathbf{e}^{(k)})^T \cdot \mathbf{e}^{(l)}, \quad k, l = 1, \dots, n \quad (\text{A3})$$

where the transpose (rather than the complex conjugate) is used to remain consistent with the c-product in complex algebra.

The linear system of size $(n + 1)$ to determine the DIIS coefficients w is

$$\begin{pmatrix} E & -\mathbf{1} \\ -\mathbf{1}^T & 0 \end{pmatrix} \begin{pmatrix} \mathbf{w} \\ \lambda \end{pmatrix} = \begin{pmatrix} 0 \\ -1 \end{pmatrix} \quad (\text{A4})$$

where $\mathbf{1}$ denotes a column vector of ones, and λ is a Lagrange multiplier enforcing the normalization condition $\sum_{k=1}^n w_i = 1$. Solving this system yields the optimal coefficients for the linear combination of previous iterations.

The extrapolated Fock matrix for the next iteration is obtained from these coefficients as

$$\mathbf{F}^{(n+1)} = \sum_{k=1}^n w_k \mathbf{F}^{(k)} \quad (\text{A5})$$

This procedure significantly enhances the convergence and stability of self-consistent HF and qsGW calculations by efficiently reducing the residual error at each iteration.

APPENDIX B

SRG Renormalization for Complex qsGW

We extended the SRG renormalization method¹⁵⁷ for complex-valued energies, which yields the following matrix elements of the self-energy

$$\begin{aligned} [\tilde{\Sigma}_c]_{pq} = & \sum_{i\nu} \frac{(\tilde{\epsilon}_{pi\nu} + \tilde{\epsilon}_{qi\nu}) N_{pq\nu}}{\tilde{\epsilon}_{pi\nu}^2 + \tilde{\epsilon}_{qi\nu}^2 + \tilde{\kappa}_{pi\nu}^2 + \tilde{\kappa}_{qi\nu}^2} \\ & + \sum_{a\nu} \frac{(\tilde{\epsilon}_{pa\nu} + \tilde{\epsilon}_{qa\nu}) N_{pq\nu}}{\tilde{\epsilon}_{pa\nu}^2 + \tilde{\epsilon}_{qa\nu}^2 + \tilde{\kappa}_{pa\nu}^2 + \tilde{\kappa}_{qa\nu}^2} \\ & + i \sum_{i\nu} \frac{(\tilde{\kappa}_{pi\nu} + \tilde{\kappa}_{qi\nu}) N_{pq\nu}}{\tilde{\epsilon}_{pi\nu}^2 + \tilde{\epsilon}_{qi\nu}^2 + \tilde{\kappa}_{pi\nu}^2 + \tilde{\kappa}_{qi\nu}^2} \\ & - i \sum_{a\nu} \frac{(\tilde{\kappa}_{pa\nu} + \tilde{\kappa}_{qa\nu}) N_{pq\nu}}{\tilde{\epsilon}_{pa\nu}^2 + \tilde{\epsilon}_{qa\nu}^2 + \tilde{\kappa}_{pa\nu}^2 + \tilde{\kappa}_{qa\nu}^2} \end{aligned} \quad (\text{B1})$$

with the real and imaginary parts of the denominator in eq 17

$$\tilde{\epsilon}_{pq\nu} = \text{Re}\{\epsilon_p - \epsilon_q - \text{sgn}[\text{Re}(\epsilon_q - \mu)]\Omega_\nu\} \quad (\text{B2a})$$

$$\tilde{\kappa}_{pq\nu} = \kappa + \text{Im}\{\text{sgn}[\text{Re}(\epsilon_q - \mu)](\epsilon_p - \epsilon_q) - \Omega_\nu\} \quad (\text{B2b})$$

(where μ is the chemical potential) and the renormalized elements

$$N_{pq\nu} = M_{pr,\nu} M_{qr,\nu} [1 - e^{-s(\tilde{\epsilon}_{pr\nu}^2 + \tilde{\epsilon}_{qr\nu}^2 + \tilde{\kappa}_{pr\nu}^2 + \tilde{\kappa}_{qr\nu}^2)}] \quad (\text{B3})$$

The exponential term in the renormalized density ensures that the numerator tends faster to zero when both the real and imaginary parts of the denominator tend to zero.

ASSOCIATED CONTENT

Supporting Information

The Supporting Information is available free of charge at <https://pubs.acs.org/doi/10.1021/acs.jctc.5c01164>.

The Supporting Information contains, for each system considered here, the molecular coordinates, the exponents of the additional diffuse basis functions, the representation of the Dyson orbital associated with the resonance state, the behavior of the energy-velocity as a function of η , and the spectral functions (PDF)

AUTHOR INFORMATION

Corresponding Author

Pierre-François Loos – Laboratoire de Chimie et Physique Quantiques (UMR 5626), Université de Toulouse, CNRS, Toulouse 31062, France; orcid.org/0000-0003-0598-7425; Email: loos@irsamc.ups-tlse.fr

Authors

Loris Burth – Laboratoire de Chimie et Physique Quantiques (UMR 5626), Université de Toulouse, CNRS, Toulouse 31062, France

Fábris Kossoski – Laboratoire de Chimie et Physique Quantiques (UMR 5626), Université de Toulouse, CNRS, Toulouse 31062, France; orcid.org/0000-0002-1627-7093

Complete contact information is available at:

<https://pubs.acs.org/10.1021/acs.jctc.5c01164>

Notes

The authors declare no competing financial interest.

ACKNOWLEDGMENTS

The authors would like to thank Josep Alberola, Antoine Marie, Ivan Duchemin, and Xavier Blase for insightful discussions. This project has received funding from the European Research Council (ERC) under the European Union's Horizon 2020 research and innovation programme (Grant agreement No. 863481). This work used the HPC resources from CALMIP (Toulouse) under allocations 2025-18005.

REFERENCES

- Jordan, K. D.; Burrow, P. D. Temporary Anion States of Polyatomic Hydrocarbons. *Chem. Rev.* **1987**, *87*, 557–588.
- Jordan, K. D.; Wang, F. Theory of Dipole-Bound Anions. *Annu. Rev. Phys. Chem.* **2003**, *54*, 367–396.
- Simons, J. Molecular Anions. *J. Phys. Chem. A* **2008**, *112*, 6401–6511.
- Simons, J. Theoretical Study of Negative Molecular Ions. *Annu. Rev. Phys. Chem.* **2011**, *62*, 107–128.
- Jordan, K. D.; Voora, V. K.; Simons, J. Negative Electron Affinities From Conventional Electronic Structure Methods. *Theor. Chem. Acc.* **2014**, *133*, 1445.
- Simons, J. Detachment Processes For Molecular Anions. In *Advanced Series in Physical Chemistry: Photoionization and Photo-detachment*; World Scientific Publishing Co.: Singapore, 2000; pp 958–1010.
- Simons, J. Molecular anions perspective. *J. Phys. Chem. A* **2023**, *127*, 3940–3957.
- Boudaïffa, B.; Cloutier, P.; Hunting, D.; Huels, M. A.; Sanche, L. Resonant Formation of DNA Strand Breaks by Low-Energy (3 to 20 eV) Electrons. *Science* **2000**, *287*, 1658–1660.
- Martin, F.; Burrow, P. D.; Cai, Z.; Cloutier, P.; Hunting, D.; Sanche, L. DNA Strand Breaks Induced by 0–4 eV Electrons: The Role of Shape Resonances. *Phys. Rev. Lett.* **2004**, *93*, 068101.
- Simons, J. How Do Low-Energy (0.1–2 eV) Electrons Cause DNA-Strand Breaks? *Acc. Chem. Res.* **2006**, *39*, 772–779.
- Alizadeh, E.; Orlando, T. M.; Sanche, L. Biomolecular Damage Induced by Ionizing Radiation: The Direct and Indirect Effects of Low-Energy Electrons on DNA. *Annu. Rev. Phys. Chem.* **2015**, *66*, 379–398.
- Hammer, N. I.; Shin, J.-W.; Headrick, J. M.; Diken, E. G.; Roscioli, J. R.; Weddle, G. H.; Johnson, M. A. How Do Small Water Clusters Bind an Excess Electron? *Science* **2004**, *306*, 675–679.

- (13) Clarke, C. J.; Verlet, J. R. Dynamics of anions: From bound to unbound states and everything in between. *Annu. Rev. Phys. Chem.* **2024**, *75*, 89–110.
- (14) Gamow, G. Zur Quantentheorie des Atomkernes. *Z. Phys.* **1928**, *51*, 204–212.
- (15) Siegert, A. J. F. On the Derivation of the Dispersion Formula for Nuclear Reactions. *Phys. Rev.* **1939**, *56*, 750–752.
- (16) Klaiman, S.; Gilary, I. On Resonance: A First Glance into the Behavior of Unstable States. *Adv. Quantum Chem.* **2012**, *63*, 1–31.
- (17) Zuev, D.; Bravaya, K. B.; Crawford, T. D.; Lindh, R.; Krylov, A. I. Electronic structure of the two isomers of the anionic form of p-coumaric acid chromophore. *J. Chem. Phys.* **2011**, *134*, 034310.
- (18) Bravaya, K. B.; Zuev, D.; Epifanovsky, E.; Krylov, A. I. Complex-Scaled Equation-Of-Motion Coupled-Cluster Method with Single and Double Substitutions for Autoionizing Excited States: Theory, Implementation, and Examples. *J. Chem. Phys.* **2013**, *138*, 124106.
- (19) Kunitsa, A. A.; Bravaya, K. B. First-Principles Calculations of the Energy and Width of the 2A_u Shape Resonance in p-Benzoquinone: A Gateway State for Electron Transfer. *J. Phys. Chem. Lett.* **2015**, *6*, 1053–1058.
- (20) Feshbach, H. Unified Theory of Nuclear Reactions. *Ann. Phys.* **1958**, *5*, 357–390.
- (21) Feshbach, H. A Unified Theory of Nuclear Reactions. II. *Ann. Phys.* **1962**, *19*, 287–313.
- (22) Domcke, W. Theory of resonance and threshold effects in electron-molecule collisions: The projection-operator approach. *Phys. Rep.* **1991**, *208*, 97–188.
- (23) Averbukh, V.; Cederbaum, L. S. Ab initio calculation of interatomic decay rates by a combination of the fano ansatz, green's-function methods, and the stieljes imaging technique. *J. Chem. Phys.* **2005**, *123*, 204107.
- (24) Kolorenč, P.; Averbukh, V.; Gokhberg, K.; Cederbaum, L. S. Ab initio calculation of interatomic decay rates of excited doubly ionized states in clusters. *J. Chem. Phys.* **2008**, *129*, 244102.
- (25) Kolorenč, J.; Mitas, L. Applications of quantum Monte Carlo methods in condensed systems. *Rep. Prog. Phys.* **2011**, *74*, 026502.
- (26) Yabushita, S.; McCurdy, C. W. Feshbach resonances in electron–molecule scattering by the complex multiconfiguration scf and configuration interaction procedures: The $^1\sigma_g^+$ autoionizing states of h₂. *J. Chem. Phys.* **1985**, *83*, 3547–3559.
- (27) Sajeev, Y.; Vysotskiy, V.; Cederbaum, L. S.; Moiseyev, N. Continuum remover-complex absorbing potential: Efficient removal of the nonphysical stabilization points. *J. Chem. Phys.* **2009**, *131*, 211102.
- (28) Schiedt, J.; Weinkauf, R. Resonant photodetachment via shape and feshbach resonances: p-benzoquinone anions as a model system. *J. Chem. Phys.* **1999**, *110*, 304–314.
- (29) Kunitsa, A. A.; Bravaya, K. B. Electronic structure of the para-benzoquinone radical anion revisited. *Phys. Chem. Chem. Phys.* **2016**, *18*, 3454–3462.
- (30) Kunitsa, A. A.; Granovsky, A. A.; Bravaya, K. B. CAP-XMCQDPT2 Method for Molecular Electronic Resonances. *J. Chem. Phys.* **2017**, *146*, 184107.
- (31) Loupas, A.; Gorfinkel, J. D. Resonances in low-energy electron scattering from para-benzoquinone. *Phys. Chem. Chem. Phys.* **2017**, *19*, 18252–18261.
- (32) da Costa, R. F.; Ruivo, J. C.; Kossofski, F.; Varella, M. T. d. N.; Bettega, M. H. F.; Jones, D. B.; Brunger, M. J.; Lima, M. A. P. An ab initio investigation for elastic and electronically inelastic electron scattering from para-benzoquinone. *J. Chem. Phys.* **2018**, *149*, 174308.
- (33) Sedmidubská, B.; Kočíšek, J. Interaction of low-energy electrons with radiosensitizers. *Phys. Chem. Chem. Phys.* **2024**, *26*, 9112–9136.
- (34) Wu, Q. T.; Anderson, H.; Watkins, A. K.; Arora, D.; Barnes, K.; Padovani, M.; Shingledecker, C. N.; Arumainayagam, C. R.; Battat, J. B. R. Role of Low-Energy (< 20 eV) Secondary Electrons in the Extraterrestrial Synthesis of Prebiotic Molecules. *ACS Earth Space Chem.* **2024**, *8*, 79–88.
- (35) Arumainayagam, C. R.; Lee, H.-L.; Nelson, R. B.; Haines, D. R.; Gunawardane, R. P. Low-energy electron-induced reactions in condensed matter. *Surf. Sci. Rep.* **2010**, *65*, 1–44.
- (36) Thorman, R. M.; Kumar T P, R.; Fairbrother, D. H.; Ingólfsson, O. The role of low-energy electrons in focused electron beam induced deposition: four case studies of representative precursors. *Beilstein J. Nanotechnol.* **2015**, *6*, 1904–1926.
- (37) Jagau, T.-C.; Bravaya, K. B.; Krylov, A. I. Extending Quantum Chemistry of Bound States to Electronic Resonances. *Annu. Rev. Phys. Chem.* **2017**, *68*, 525–553.
- (38) Jagau, T.-C. Theory of electronic resonances: fundamental aspects and recent advances. *Chem. Commun.* **2022**, *58*, 5205–5224.
- (39) Jolicard, G.; Austin, E. J. Optical potential stabilisation method for predicting resonance levels. *Chem. Phys. Lett.* **1985**, *121*, 106–110.
- (40) Riss, U. V.; Meyer, H.-D. Calculation of resonance energies and widths using the complex absorbing potential method. *J. Phys. B: At., Mol. Opt. Phys.* **1993**, *26*, 4503.
- (41) Sommerfeld, T.; Riss, U. V.; Meyer, H.-D.; Cederbaum, L. S.; Engels, B.; Suter, H. U. Temporary anions - calculation of energy and lifetime by absorbing potentials: the resonance. *J. Phys. B: At., Mol. Opt. Phys.* **1998**, *31*, 4107.
- (42) Ghosh, A.; Vaval, N.; Pal, S. Equation-of-motion coupled-cluster method for the study of shape resonance. *J. Chem. Phys.* **2012**, *136*, 234110.
- (43) Zuev, D.; Jagau, T.-C.; Bravaya, K. B.; Epifanovsky, E.; Shao, Y.; Sundstrom, E.; Head-Gordon, M.; Krylov, A. I. Complex Absorbing Potentials Within EOM-CC Family of Methods: Theory, Implementation, and Benchmarks. *J. Chem. Phys.* **2014**, *141*, 024102.
- (44) Jagau, T.-C.; Zuev, D.; Bravaya, K. B.; Epifanovsky, E.; Krylov, A. I. A Fresh Look at Resonances and Complex Absorbing Potentials: Density Matrix-Based Approach. *J. Phys. Chem. Lett.* **2014**, *5*, 310–315.
- (45) Jagau, T.-C.; Krylov, A. I. Complex Absorbing Potential Equation-of-Motion Coupled-Cluster Method Yields Smooth and Internally Consistent Potential Energy Surfaces and Lifetimes for Molecular Resonances. *J. Phys. Chem. Lett.* **2014**, *5*, 3078–3085.
- (46) Sommerfeld, T.; Ehara, M. Complex absorbing potentials with voronoi isosurfaces wrapping perfectly around molecules. *J. Chem. Theory Comput.* **2015**, *11*, 4627–4633.
- (47) Gyamfi, J. A.; Jagau, T.-C. A New Strategy to Optimize Complex Absorbing Potentials for the Computation of Resonance Energies and Widths. *J. Chem. Theory Comput.* **2024**, *20*, 1096–1107.
- (48) Balslev, E.; Combes, J. M. Spectral properties of many-body Schrödinger operators with dilatation-analytic interactions. *Commun. Math. Phys.* **1971**, *22*, 280–294.
- (49) Moiseyev, N. Quantum theory of resonances: calculating energies, widths and cross-sections by complex scaling. *Phys. Rep.* **1998**, *302*, 212–293.
- (50) McCurdy, C. W.; Rescigno, T. N. Extension of the method of complex basis functions to molecular resonances. *Phys. Rev. Lett.* **1978**, *41*, 1364–1368.
- (51) White, A. F.; Head-Gordon, M.; McCurdy, C. W. Complex basis functions revisited: Implementation with applications to carbon tetrafluoride and aromatic N-containing heterocycles within the static-exchange approximation. *J. Chem. Phys.* **2015**, *142*, 054103.
- (52) Moiseyev, N. *Non-Hermitian Quantum Mechanics*; Cambridge University Press: Cambridge, England, UK, 2011.
- (53) Damour, Y.; Scemama, A.; Kossofski, F.; Loos, P.-F. Selected Configuration Interaction for Resonances. *J. Phys. Chem. Lett.* **2024**, *15*, 8296–8305.
- (54) Ghosh, A.; Karne, A.; Pal, S.; Vaval, N. CAP/EOM-CCSD method for the study of potential curves of resonant states. *Phys. Chem. Chem. Phys.* **2013**, *15*, 17915–17921.
- (55) Sajeev, Y.; Santra, R.; Pal, S. Analytically continued Fock space multireference coupled-cluster theory: Application to the Πg_2 shape resonance in e-N₂ scattering. *J. Chem. Phys.* **2005**, *122*, 234320.
- (56) Sajeev, Y.; Pal, S. A general formalism of the Fock space multireference coupled cluster method for investigating molecular electronic resonances. *Mol. Phys.* **2005**, *103*, 2267–2275.

- (57) Jagau, T.-C. Non-iterative triple excitations in equation-of-motion coupled-cluster theory for electron attachment with applications to bound and temporary anions. *J. Chem. Phys.* **2018**, *148*, 024104.
- (58) Jana, I.; Basumallick, S.; Pal, S.; Vaval, N. Resonance study: Effect of partial triples excitation using complex absorbing potential-based Fock-space multi-reference coupled cluster. *Int. J. Quantum Chem.* **2021**, *121*, No. e26738.
- (59) Ehara, M.; Sommerfeld, T. CAP/SAC-CI method for calculating resonance states of metastable anions. *Chem. Phys. Lett.* **2012**, *537*, 107–112.
- (60) Phung, Q. M.; Komori, Y.; Yanai, T.; Sommerfeld, T.; Ehara, M. Combination of a Voronoi-Type Complex Absorbing Potential with the XMS-CASPT2 Method and Pilot Applications. *J. Chem. Theory Comput.* **2020**, *16*, 2606–2616.
- (61) Sommerfeld, T.; Santra, R. Efficient method to perform CAP/CI calculations for temporary anions. *Int. J. Quantum Chem.* **2001**, *82*, 218–226.
- (62) Zhou, Y.; Ernzerhof, M. Calculating the lifetimes of metastable states with complex density functional theory. *J. Phys. Chem. Lett.* **2012**, *3*, 1916–1920.
- (63) Gayvert, J. R.; Bravaya, K. B. Projected CAP-EOM-CCSD method for electronic resonances. *J. Chem. Phys.* **2022**, *156*, 094108.
- (64) Santra, R.; Cederbaum, L. S. Complex absorbing potentials in the framework of electron propagator theory. I. General formalism. *J. Chem. Phys.* **2002**, *117*, 5511–5521.
- (65) Feuerbacher, S.; Sommerfeld, T.; Santra, R.; Cederbaum, L. S. Complex absorbing potentials in the framework of electron propagator theory. II. Application to temporary anions. *J. Chem. Phys.* **2003**, *118*, 6188–6199.
- (66) Feuerbacher, S.; Santra, R. Calculating molecular Rydberg states using the one-particle Green's function: Application to HCO and C(NH₂)₃. *J. Chem. Phys.* **2005**, *123*, 194310.
- (67) Belogolova, A. M.; Dempwolff, A. L.; Dreuw, A.; Trofimov, A. B. A complex absorbing potential electron propagator approach to resonance states of metastable anions. *J. Phys.: Conf. Ser.* **2021**, *1847*, 012050.
- (68) Dempwolff, A. L.; Belogolova, A. M.; Sommerfeld, T.; Trofimov, A. B.; Dreuw, A. Cap/ea-adc method for metastable anions: Computational aspects and application to π^* resonances of norbornadiene and 1,4-cyclohexadiene. *J. Chem. Phys.* **2021**, *155*, 054103.
- (69) Schirmer, J.; Trofimov, A. B.; Stelter, G. A non-Dyson third-order approximation scheme for the electron propagator. *J. Chem. Phys.* **1998**, *109*, 4734–4744.
- (70) Schirmer, J. *Many-Body Methods for Atoms, Molecules and Clusters*; Springer, 2018.
- (71) Martin, R. M.; Reining, L.; Ceperley, D. M. *Interacting Electrons: Theory and Computational Approaches*; Cambridge University Press, 2016.
- (72) Csanak, G.; Taylor, H.; Yaris, R. Green's function technique in atomic and molecular physics. *Adv. At. Mol. Phys.* **1971**, *7*, 287–361.
- (73) Fetter, A. L.; Waleck, J. D. *Quantum Theory of Many Particle Systems*; McGraw Hill: San Francisco, 1971.
- (74) Hedin, L. New method for calculating the one-particle Green's function with application to the electron-gas problem. *Phys. Rev.* **1965**, *139*, A796.
- (75) Golze, D.; Dvorak, M.; Rinke, P. The GW Compendium: A Practical Guide to Theoretical Photoemission Spectroscopy. *Front. Chem.* **2019**, *7*, 377.
- (76) Marie, A.; Ammar, A.; Loos, P.-F. The GW approximation: A quantum chemistry perspective. *Adv. Quantum Chem.* **2024**, *90*, 157–184.
- (77) Falsetta, M. F.; DiFalco, L. A.; Ackerman, D. S.; Barlow, J. C.; Jordan, K. D. Assessment of various electronic structure methods for characterizing temporary anion states: Application to the ground state anions of n₂, c2h₂, c2h₄, and c6h₆. *J. Phys. Chem. A* **2014**, *118*, 7489–7497.
- (78) Hazi, A. U.; Taylor, H. S. Stabilization Method of Calculating Resonance Energies: Model Problem. *Phys. Rev. A* **1970**, *1*, 1109–1120.
- (79) van Setten, M. J.; Caruso, F.; Sharifzadeh, S.; Ren, X.; Scheffler, M.; Liu, F.; Lischner, J.; Lin, L.; Deslippe, J. R.; Louie, S. G.; Yang, C.; Weigend, F.; Neaton, J. B.; Evers, F.; Rinke, P. GW 100: Benchmarking G_0W_0 for Molecular Systems. *J. Chem. Theory Comput.* **2015**, *11*, 5665–5687.
- (80) Caruso, F.; Dauth, M.; van Setten, M. J.; Rinke, P. Benchmark of GW Approaches for the GW100 Test Set. *J. Chem. Theory Comput.* **2016**, *12*, 5076.
- (81) Krause, K.; Klopper, W. Implementation of the bethe-salpeter equation in the turbomole program. *J. Comput. Chem.* **2017**, *38*, 383–388.
- (82) Lewis, A. M.; Berkelbach, T. C. Vertex corrections to the polarizability do not improve the GW approximation for the ionization potential of molecules. *J. Chem. Theory Comput.* **2019**, *15*, 2925.
- (83) Bruneval, F.; Dattani, N.; van Setten, M. J. The GW Miracle in Many-Body Perturbation Theory for the Ionization Potential of Molecules. *Front. Chem.* **2021**, *9*, 749779.
- (84) Monino, E.; Loos, P.-F. Connections and performances of green's function methods for charged and neutral excitations. *J. Chem. Phys.* **2023**, *159*, 034105.
- (85) Marie, A.; Loos, P.-F. Reference Energies for Valence Ionizations and Satellite Transitions. *J. Chem. Theory Comput.* **2024**, *20*, 4751–4777.
- (86) van Setten, M. J.; Costa, R.; Viñes, F.; Illas, F. Assessing GW Approaches for Predicting Core Level Binding Energies. *J. Chem. Theory Comput.* **2018**, *14*, 877–883.
- (87) Golze, D.; Wilhelm, J.; van Setten, M. J.; Rinke, P. Core-Level Binding Energies from GW: An Efficient Full-Frequency Approach within a Localized Basis. *J. Chem. Theory Comput.* **2018**, *14*, 4856–4869.
- (88) Golze, D.; Keller, L.; Rinke, P. Accurate Absolute and Relative Core-Level Binding Energies from GW. *J. Phys. Chem. Lett.* **2020**, *11*, 1840–1847.
- (89) Mejia-Rodriguez, D.; Kunitsa, A.; Aprà, E.; Govind, N. Scalable Molecular GW Calculations: Valence and Core Spectra. *J. Chem. Theory Comput.* **2021**, *17*, 7504–7517.
- (90) Li, J.; Jin, Y.; Rinke, P.; Yang, W.; Golze, D. Benchmark of GW methods for core-level binding energies. *J. Chem. Theory Comput.* **2022**, *18*, 7570–7585.
- (91) Mukatayev, I.; Moevus, F.; Sklénard, B.; Olevano, V.; Li, J. XPS Core-Level Chemical Shift by Ab Initio Many-Body Theory. *J. Phys. Chem. A* **2023**, *127*, 1642–1648.
- (92) Panades-Barrueta, R. L.; Golze, D. Accelerating Core-Level GW Calculations by Combining the Contour Deformation Approach with the Analytic Continuation of W. *J. Chem. Theory Comput.* **2023**, *19*, 5450–5464.
- (93) Baym, G.; Kadanoff, L. P. Conservation laws and correlation functions. *Phys. Rev.* **1961**, *124*, 287–299.
- (94) Baym, G. Self-consistent approximations in many-body systems. *Phys. Rev.* **1962**, *127*, 1391–1401.
- (95) De Dominicis, C.; Martin, P. C. Stationary entropy principle and renormalization in normal and superfluid systems. i. algebraic formulation. *J. Math. Phys.* **1964**, *5*, 14–30.
- (96) De Dominicis, C.; Martin, P. C. Stationary entropy principle and renormalization in normal and superfluid systems. ii. diagrammatic formulation. *J. Math. Phys.* **1964**, *5*, 31–59.
- (97) Bickers, N. E.; Scalapino, D. J.; White, S. R. Conserving Approximations for Strongly Correlated Electron Systems: Bethe-Salpeter Equation and Dynamics for the Two-Dimensional Hubbard Model. *Phys. Rev. Lett.* **1989**, *62*, 961–964.
- (98) Bickers, N.; Scalapino, D. Conserving approximations for strongly fluctuating electron systems. I. Formalism and calculational approach. *Ann. Phys.* **1989**, *193*, 206–251.
- (99) Bickers, N. E.; White, S. R. Conserving approximations for strongly fluctuating electron systems. II. Numerical results and

- parquet extension. *Phys. Rev. B: Condens. Matter Mater. Phys.* **1991**, *43*, 8044–8064.
- (100) Hedin, L. On correlation effects in electron spectroscopies and the *GW* approximation. *J. Phys.: Condens. Matter* **1999**, *11*, R489–R528.
- (101) Bickers, N. E. Self-Consistent Many-Body Theory for Condensed Matter Systems. In *Theoretical Methods for Strongly Correlated Electrons*; Sénechal, D., Tremblay, A.-M., Bourbonnais, C., Eds.; Springer New York: New York, NY, 2004; pp 237–296.
- (102) Shirley, E. L. Self-consistent *GW* and higher-order calculations of electron states in metals. *Phys. Rev. B: Condens. Matter Mater. Phys.* **1996**, *54*, 7758–7764.
- (103) Del Sole, R.; Reining, L.; Godby, R. W. *GWT* Approximation for Electron Self-Energies in Semiconductors and Insulators. *Phys. Rev. B: Condens. Matter Mater. Phys.* **1994**, *49*, 8024–8028.
- (104) Schindlmayr, A.; Godby, R. W. Systematic Vertex Corrections through Iterative Solution of Hedin's Equations Beyond the *GW* Approximation. *Phys. Rev. Lett.* **1998**, *80*, 1702–1705.
- (105) Morris, A. J.; Stankovski, M.; Delaney, K. T.; Rinke, P.; García-González, P.; Godby, R. W. Vertex corrections in localized and extended systems. *Phys. Rev. B: Condens. Matter Mater. Phys.* **2007**, *76*, 155106.
- (106) Shishkin, M.; Marsman, M.; Kresse, G. Accurate Quasiparticle Spectra from Self-Consistent *GW* Calculations with Vertex Corrections. *Phys. Rev. Lett.* **2007**, *99*, 246403.
- (107) Romaniello, P.; Guyot, S.; Reining, L. The self-energy beyond *GW*: Local and nonlocal vertex corrections. *J. Chem. Phys.* **2009**, *131*, 154111.
- (108) Romaniello, P.; Bechstedt, F.; Reining, L. Beyond the *GW* Approximation: Combining Correlation Channels. *Phys. Rev. B: Condens. Matter Mater. Phys.* **2012**, *85*, 155131.
- (109) Grüneis, A.; Kresse, G.; Hinuma, Y.; Oba, F. Ionization potentials of solids: The importance of vertex corrections. *Phys. Rev. Lett.* **2014**, *112*, 096401.
- (110) Hung, L.; Bruneval, F.; Baishya, K.; Öğüt, S. Benchmarking the *GW* Approximation and Bethe–Salpeter Equation for Groups IB and IIB Atoms and Monoxides. *J. Chem. Theory Comput.* **2017**, *13*, 2135–2146.
- (111) Maggio, E.; Kresse, G. *GW* Vertex Corrected Calculations for Molecular Systems. *J. Chem. Theory Comput.* **2017**, *13*, 4765–4778.
- (112) Mejuto-Zaera, C.; Vlcek, V. c. v. Self-consistency in *GWT* formalism leading to quasiparticle-quasiparticle couplings. *Phys. Rev. B* **2022**, *106*, 165129.
- (113) Wen, M.; Abraham, V.; Harsha, G.; Shee, A.; Whaley, K. B.; Zgid, D. Comparing Self-Consistent *GW* and Vertex-Corrected G_0W_0 ($G_0W_0\Gamma$) Accuracy for Molecular Ionization Potentials. *J. Chem. Theory Comput.* **2024**, *20*, 3109–3120.
- (114) Bruneval, F.; Förster, A. Fully Dynamic *G3W2* Self-Energy for Finite Systems: Formulas and Benchmark. *J. Chem. Theory Comput.* **2024**, *20*, 3218–3230.
- (115) Förster, A.; Bruneval, F. Why Does the *GW* Approximation Give Accurate Quasiparticle Energies? The Cancellation of Vertex Corrections Quantified. *J. Phys. Chem. Lett.* **2024**, *15*, 12526–12534.
- (116) Förster, A. Beyond Quasi-Particle Self-Consistent *GW* for Molecules with Vertex Corrections. *J. Chem. Theory Comput.* **2025**, *21*, 1709–1721.
- (117) Neuhauser, D.; Rabani, E.; Baer, R. Expedited stochastic calculation of random-phase approximation energies for thousands of electrons in three dimensions. *J. Phys. Chem. Lett.* **2013**, *4*, 1172–1176.
- (118) Neuhauser, D.; Gao, Y.; Arntsen, C.; Karshenas, C.; Rabani, E.; Baer, R. Breaking the Theoretical Scaling Limit for Predicting Quasiparticle Energies: The Stochastic *GW* Approach. *Phys. Rev. Lett.* **2014**, *113*, 076402.
- (119) Kaltak, M.; Klimeš, J.; Kresse, G. Low scaling algorithms for the random phase approximation: Imaginary time and laplace transformations. *J. Chem. Theory Comput.* **2014**, *10*, 2498–2507.
- (120) Govoni, M.; Galli, G. Large Scale *GW* Calculations. *J. Chem. Theory Comput.* **2015**, *11*, 2680–2696.
- (121) Vlček, V.; Rabani, E.; Neuhauser, D.; Baer, R. Stochastic *GW* Calculations for Molecules. *J. Chem. Theory Comput.* **2017**, *13*, 4997–5003.
- (122) Wilhelm, J.; Golze, D.; Talirz, L.; Hutter, J.; Pignedoli, C. A. Toward *GW* Calculations on Thousands of Atoms. *J. Phys. Chem. Lett.* **2018**, *9*, 306–312.
- (123) Duchemin, I.; Blase, X. Separable resolution-of-the-identity with all-electron gaussian bases: Application to cubic-scaling rpa. *J. Chem. Phys.* **2019**, *150*, 174120.
- (124) Ben, M. D.; da Jornada, F. H.; Canning, A.; Wichmann, N.; Raman, K.; Sasanka, R.; Yang, C.; Louie, S. G.; Deslippe, J. Large-scale *GW* calculations on pre-exascale HPC systems. *Comput. Phys. Commun.* **2019**, *235*, 187–195.
- (125) Förster, A.; Visscher, L. Low-Order Scaling *G0W0* by Pair Atomic Density Fitting. *J. Chem. Theory Comput.* **2020**, *16*, 7381–7399.
- (126) Duchemin, I.; Blase, X. Robust analytic-continuation approach to many-body *GW* calculations. *J. Chem. Theory Comput.* **2020**, *16*, 1742–1756.
- (127) Kaltak, M.; Kresse, G. Minimax isometry method: A compressive sensing approach for matsubara summation in many-body perturbation theory. *Phys. Rev. B* **2020**, *101*, 205145.
- (128) Förster, A.; Visscher, L. Low-Order Scaling Quasiparticle Self-Consistent *GW* for Molecules. *Front. Chem.* **2021**, *9*, 736591.
- (129) Duchemin, I.; Blase, X. Cubic-scaling all-electron *GW* calculations with a separable density-fitting space–time approach. *J. Chem. Theory Comput.* **2021**, *17*, 2383–2393.
- (130) Wilhelm, J.; Seewald, P.; Golze, D. Low-Scaling *GW* with Benchmark Accuracy and Application to Phosphorene Nanosheets. *J. Chem. Theory Comput.* **2021**, *17*, 1662–1677.
- (131) Förster, A.; Visscher, L. Quasiparticle Self-Consistent *GW*-Bethe–Salpeter Equation Calculations for Large Chromophoric Systems. *J. Chem. Theory Comput.* **2022**, *18*, 6779–6793.
- (132) Yu, V. W.-z.; Govoni, M. GPU Acceleration of Large-Scale Full-Frequency *GW* Calculations. *J. Chem. Theory Comput.* **2022**, *18*, 4690–4707.
- (133) Tölle, J.; Niemeyer, N.; Neugebauer, J. Accelerating analytic-continuation *GW* calculations with a laplace transform and natural auxiliary functions. *J. Chem. Theory Comput.* **2024**, *20*, 2022–2032.
- (134) Krause, K.; Harding, M. E.; Klopper, W. Coupled-Cluster Reference Values For The *GW27* And *GW100* Test Sets For The Assessment Of *GW* Methods. *Mol. Phys.* **2015**, *113*, 1952.
- (135) Richard, R. M.; Marshall, M. S.; Dolgounitcheva, O.; Ortiz, J. V.; Brédas, J.-L.; Marom, N.; Sherrill, C. D. Accurate Ionization Potentials and Electron Affinities of Acceptor Molecules I. Reference Data at the CCSD(T) Complete Basis Set Limit. *J. Chem. Theory Comput.* **2016**, *12*, 595–604.
- (136) Knight, J. W.; Wang, X.; Gallandi, L.; Dolgounitcheva, O.; Ren, X.; Ortiz, J. V.; Rinke, P.; Körzdörfer, T.; Marom, N. Accurate Ionization Potentials and Electron Affinities of Acceptor Molecules III: A Benchmark of *GW* Methods. *J. Chem. Theory Comput.* **2016**, *12*, 615–626.
- (137) Rangel, T.; Hamed, S. M.; Bruneval, F.; Neaton, J. B. Evaluating the *GW* Approximation with CCSD(T) for Charged Excitations Across the Oligoacenes. *J. Chem. Theory Comput.* **2016**, *12*, 2834–2842.
- (138) Förster, A.; Visscher, L. Exploring the statically screened *G3W2* correction to the *GW* self-energy: Charged excitations and total energies of finite systems. *Phys. Rev. B* **2022**, *105*, 125121.
- (139) Ghosal, A.; Joshi, P.; Voora, V. K. Taming negative ion resonances using nonlocal exchange-correlation functionals. *J. Phys. Chem. Lett.* **2024**, *15*, 5994–6001.
- (140) Strinati, G.; Mattausch, H. J.; Hanke, W. Dynamical correlation effects on the quasiparticle bloch states of a covalent crystal. *Phys. Rev. Lett.* **1980**, *45*, 290–294.
- (141) Hybertsen, M. S.; Louie, S. G. First-Principles Theory of Quasiparticles: Calculation of Band Gaps in Semiconductors and Insulators. *Phys. Rev. Lett.* **1985**, *55*, 1418–1421.

- (142) Godby, R. W.; Schlüter, M.; Sham, L. J. Self-energy operators and exchange-correlation potentials in semiconductors. *Phys. Rev. B: Condens. Matter Mater. Phys.* **1988**, *37*, 10159–10175.
- (143) von der Linden, W.; Horsch, P. Precise quasiparticle energies and hartree-fock bands of semiconductors and insulators. *Phys. Rev. B: Condens. Matter Mater. Phys.* **1988**, *37*, 8351–8362.
- (144) Northrup, J. E.; Hybertsen, M. S.; Louie, S. G. Many-body Calculation of the Surface-State Energies for Si(111)2 × 1. *Phys. Rev. Lett.* **1991**, *66*, 500–503.
- (145) Blase, X.; Zhu, X.; Louie, S. G. Self-energy effects on the surface-state energies of h-si(111)1 × 1. *Phys. Rev. B: Condens. Matter Mater. Phys.* **1994**, *49*, 4973–4980.
- (146) Rohlfing, M.; Krüger, P.; Pollmann, J. Efficient Scheme for GW Quasiparticle Band-Structure Calculations with Applications to Bulk Si and to the Si(001)-(2 × 1) Surface. *Phys. Rev. B: Condens. Matter Mater. Phys.* **1995**, *52*, 1905–1917.
- (147) Hybertsen, M. S.; Louie, S. G. Electron correlation in semiconductors and insulators: Band gaps and quasiparticle energies. *Phys. Rev. B: Condens. Matter Mater. Phys.* **1986**, *34*, 5390–5413.
- (148) Shishkin, M.; Kresse, G. Self-Consistent GW Calculations for Semiconductors and Insulators. *Phys. Rev. B: Condens. Matter Mater. Phys.* **2007**, *75*, 235102.
- (149) Blase, X.; Attaccalite, C. Charge-transfer excitations in molecular donor-acceptor complexes within the many-body bethe-salpeter approach. *Appl. Phys. Lett.* **2011**, *99*, 171909.
- (150) Faber, C.; Attaccalite, C.; Olevano, V.; Runge, E.; Blase, X. First-principles GW calculations for DNA and RNA nucleobases. *Phys. Rev. B: Condens. Matter Mater. Phys.* **2011**, *83*, 115123.
- (151) Gui, X.; Holzer, C.; Klopper, W. Accuracy assessment of GW starting points for calculating molecular excitation energies using the bethe-salpeter formalism. *J. Chem. Theory Comput.* **2018**, *14*, 2127–2136.
- (152) Faleev, S. V.; van Schilfgaarde, M.; Kotani, T. All-Electron Self-Consistent G W Approximation: Application to Si, MnO, and NiO. *Phys. Rev. Lett.* **2004**, *93*, 126406.
- (153) van Schilfgaarde, M.; Kotani, T.; Faleev, S. Quasiparticle Self-Consistent G W Theory. *Phys. Rev. Lett.* **2006**, *96*, 226402.
- (154) Kotani, T.; van Schilfgaarde, M.; Faleev, S. V. Quasiparticle self-consistent G W method: A basis for the independent-particle approximation. *Phys. Rev. B: Condens. Matter Mater. Phys.* **2007**, *76*, 165106.
- (155) Ke, S.-H. All-electron G W methods implemented in molecular orbital space: Ionization energy and electron affinity of conjugated molecules. *Phys. Rev. B: Condens. Matter Mater. Phys.* **2011**, *84*, 205415.
- (156) Kaplan, F.; Harding, M. E.; Seiler, C.; Weigend, F.; Evers, F.; van Setten, M. J. Quasi-Particle Self-Consistent GW for Molecules. *J. Chem. Theory Comput.* **2016**, *12*, 2528–2541.
- (157) Marie, A.; Loos, P.-F. A Similarity Renormalization Group Approach to Green's Function Methods. *J. Chem. Theory Comput.* **2023**, *19*, 3943–3957.
- (158) Moiseyev, N.; Certain, P. R.; Weinhold, F. Resonance properties of complex-rotated hamiltonians. *Mol. Phys.* **1978**, *36*, 1613–1630.
- (159) Landau, A.; Moiseyev, N. Molecular resonances by removing complex absorbing potentials via Padé; Application to CO⁻ and N₂⁻. *J. Chem. Phys.* **2016**, *145*, 164111.
- (160) Let $\tilde{C}(\eta)$ be the matrix of nonorthonormal eigenvectors, i.e., the results of a diagonalisation method for non-Hermitian complex matrices. Then, to ensure the normalization condition, we perform an adapted Cholesky decomposition to get a lower triangular matrix L fulfilling $\tilde{C}(\eta)^T \cdot S \cdot \tilde{C}(\eta) = L \cdot L^T$. Then, to obtain the orthonormalized eigenvectors, we transform the original coefficients matrix using the inverse transpose of the Cholesky factor L , as follows: $C(\eta) = \tilde{C}(\eta) \cdot L^{-T}$.
- (161) Santra, R.; Cederbaum, L.; Meyer, H.-D. Electronic decay of molecular clusters: non-stationary states computed by standard quantum chemistry methods. *Chem. Phys. Lett.* **1999**, *303*, 413–419.
- (162) Aryasetiawan, F.; Gunnarsson, O. The GW Method. *Rep. Prog. Phys.* **1998**, *61*, 237–312.
- (163) Onida, G.; Reining, L.; Rubio, A. Electronic excitations: Density-functional versus many-body green's function approaches. *Rev. Mod. Phys.* **2002**, *74*, 601–659.
- (164) Reining, L. The GW Approximation: Content, Successes and Limitations. *Wiley Interdiscip. Rev.: Comput. Mol. Sci.* **2017**, *8*, No. e1344.
- (165) DickHoff, W. H.; Neck, D. V. *Many-Body Theory Exposed!*; World Scientific, 2008.
- (166) Starke, R.; Kresse, G. Self-consistent Green function equations and the hierarchy of approximations for the four-point propagator. *Phys. Rev. B: Condens. Matter Mater. Phys.* **2012**, *85*, 075119.
- (167) Orlando, R.; Romaniello, P.; Loos, P.-F. The three channels of many-body perturbation theory: GW, particle–particle, and electron–hole T-matrix self-energies. *J. Chem. Phys.* **2023**, *159*, 184113.
- (168) Marie, A.; Romaniello, P.; Loos, P.-F. Anomalous propagators and the particle-particle channel: Hedin's equations. *Phys. Rev. B* **2024**, *110*, 115155.
- (169) Marie, A.; Romaniello, P.; Blase, X.; Loos, P.-F. Anomalous propagators and the particle–particle channel: Bethe–Salpeter equation. *J. Chem. Phys.* **2025**, *162*, 134105.
- (170) Casida, M. E. *Time-Dependent Density Functional Response Theory for Molecules*; World Scientific: Singapore, 1995; pp 155–192.
- (171) Bohm, D.; Pines, D. A Collective Description of Electron Interactions. I. Magnetic Interactions. *Phys. Rev.* **1951**, *82*, 625–634.
- (172) Pines, D.; Bohm, D. A Collective Description of Electron Interactions: II. Collective vs Individual Particle Aspects of the Interactions. *Phys. Rev.* **1952**, *85*, 338–353.
- (173) Bohm, D.; Pines, D. A Collective Description of Electron Interactions: III. Coulomb Interactions in a Degenerate Electron Gas. *Phys. Rev.* **1953**, *92*, 609–625.
- (174) Nozières, P.; Pines, D. Correlation Energy of a Free Electron Gas. *Phys. Rev.* **1958**, *111*, 442–454.
- (175) Holzer, C.; Teale, A. M.; Hampe, F.; Stopkowicz, S.; Helgaker, T.; Klopper, W. GW Quasiparticle Energies of Atoms in Strong Magnetic Fields. *J. Chem. Phys.* **2019**, *150*, 214112.
- (176) Practically, we ensure the normalization of the RPA eigenvectors with the same method as introduced in the HF section, i.e., by a Cholesky decomposition of $(\begin{smallmatrix} X & Y \\ Y & X \end{smallmatrix})^T \cdot (\begin{smallmatrix} 1 & 0 \\ 0 & 1 \end{smallmatrix}) \cdot (\begin{smallmatrix} X & Y \\ Y & X \end{smallmatrix})$.
- (177) Lei, J.; Zhu, T. Gaussian-based quasiparticle self-consistent GW for periodic systems. *J. Chem. Phys.* **2022**, *157*, 214114.
- (178) Harsha, G.; Abraham, V.; Wen, M.; Zgid, D. Quasiparticle and fully self-consistent GW methods: An unbiased analysis using gaussian orbitals. *Phys. Rev. B* **2024**, *110*, 235146.
- (179) Szabo, A.; Ostlund, N. S. *Modern Quantum Chemistry*; McGraw-Hill: New York, 1989.
- (180) Loos, P. F. *QuAcK: A Software for Emerging Quantum Electronic Structure Methods*; GitHub, Inc., 2019. <https://github.com/pfloos/QuAcK>.
- (181) Gayvert, J., *OpenCap: An Open-Source Program for Studying Resonances in Molecules*; MolSSI, 2024, commit: 1562fce. Accessed: 2025-04-28.
- (182) Pulay, P. Convergence Acceleration of Iterative Sequences. The Case of SCF Iteration. *Chem. Phys. Lett.* **1980**, *73*, 393–398.
- (183) Pulay, P. Improved SCF convergence acceleration. *J. Comput. Chem.* **1982**, *3*, 556–560.
- (184) Vérit, M.; Romaniello, P.; Berger, J. A.; Loos, P. F. Unphysical discontinuities in GW methods. *J. Chem. Theory Comput.* **2018**, *14*, S220.
- (185) Nestmann, B. M.; Peyerimhoff, S. D. CI method for determining the location and width of resonances in electron-molecule collision processes. *J. Phys. B: At., Mol. Opt. Phys.* **1985**, *18*, 4309.
- (186) Vérit, M.; Scemama, A.; Caffarel, M.; Lipparini, F.; Boggio-Pasqua, M.; Jacquemin, D.; Loos, P.-F. QUESTDB: A database of highly accurate excitation energies for the electronic structure

- community. *Wiley Interdiscip. Rev.: Comput. Mol. Sci.* **2021**, *11*, No. e1517.
- (187) Jagau, T.-C.; Krylov, A. I. Characterizing metastable states beyond energies and lifetimes: Dyson orbitals and transition dipole moments. *J. Chem. Phys.* **2016**, *144*, 054113.
- (188) Camps, S.; Utku, C.; Creutzberg, J.; Jagau, T.-C. Complex-variable equation-of-motion coupled-cluster singles and doubles theory with the resolution-of-the-identity approximation. *J. Phys. Chem. A* **2025**, *129*, 4798–4811.
- (189) Berman, M.; Estrada, H.; Cederbaum, L. S.; Domcke, W. Nuclear dynamics in resonant electron-molecule scattering beyond the local approximation: The 2.3-eV shape resonance in N₂. *Phys. Rev. A* **1983**, *28*, 1363–1381.
- (190) Ehrhardt, H.; Langhans, L.; Linder, F.; Taylor, H. S. Resonance Scattering of Slow Electrons from H₂ and CO Angular Distributions. *Phys. Rev.* **1968**, *173*, 222–230.
- (191) Zubek, M.; Szmytkowski, C. Calculation of resonant vibrational excitation of CO by scattering of electrons. *J. Phys. B: At., Mol. Opt. Phys.* **1977**, *10*, L27.
- (192) Zubek, M.; Szmytkowski, C. Electron impact vibrational excitation of CO in the range 1–4 eV. *Phys. Lett. A* **1979**, *74*, 60–62.
- (193) Buckman, S. J.; Lohmann, B. Electron scattering from co in the ²Π resonance region. *Phys. Rev. A* **1986**, *34*, 1561–1563.
- (194) Szmytkowski, C.; Maciąg, K.; Karwasz, G. Absolute electron-scattering total cross section measurements for noble gas atoms and diatomic molecules. *Phys. Scr.* **1996**, *54*, 271.
- (195) Allan, M. Electron collisions with co: Elastic and vibrational excitation cross sections. *Phys. Rev. A* **2010**, *81*, 042706.
- (196) Kochem, K. H.; Sohn, W.; Jung, K.; Ehrhardt, H.; Chang, E. S. Direct and resonant vibrational excitation of C₂H₂ by electron impact from 0 to 3.6 eV. *J. Phys. B: At., Mol. Opt. Phys.* **1985**, *18*, 1253.
- (197) Jordan, K. D.; Burrow, P. D. Studies of the Temporary Anion States of Unsaturated Hydrocarbons by Electron Transmission Spectroscopy. *Acc. Chem. Res.* **1978**, *11*, 341–348.
- (198) Dressler, R.; Allan, M. A dissociative electron attachment, electron transmission, and electron energy-loss study of the temporary negative ion of acetylene. *J. Chem. Phys.* **1987**, *87*, 4510–4518.
- (199) Andric, L.; Hall, R. I. Resonance phenomena observed in electron scattering from acetylene. *J. Phys. B: At., Mol. Opt. Phys.* **1988**, *21*, 355.
- (200) Szmytkowski, C.; Możejko, P.; Zawadzki, M.; Maciąg, K.; Ptasińska-Denga, E. Electron-scattering cross sections for selected alkyne molecules: Measurements and calculations. *Phys. Rev. A* **2014**, *89*, 052702.
- (201) Benda, Z.; Rickmeyer, K.; Jagau, T.-C. Structure Optimization of Temporary Anions. *J. Chem. Theory Comput.* **2018**, *14*, 3468–3478.
- (202) Sanche, L.; Schulz, G. J. Electron transmission spectroscopy: Resonances in triatomic molecules and hydrocarbons. *J. Chem. Phys.* **1973**, *58*, 479–493.
- (203) Walker, I. C.; Stamatovic, A.; Wong, S. F. Vibrational excitation of ethylene by electron impact: 1–11 eV. *J. Chem. Phys.* **1978**, *69*, 5532–5537.
- (204) Lunt, S. L.; Randell, J.; Ziesel, J. P.; Mrotzek, G.; Field, D. Low-energy electron scattering from ch₄, c₂h₄ and c₂h₆. *J. Phys. B: At., Mol. Opt. Phys.* **1994**, *27*, 1407.
- (205) Panajotovic, R.; Kitajima, M.; Tanaka, H.; Jelisavcic, M.; Lower, J.; Campbell, L.; Brunger, M. J.; Buckman, S. J. Electron collisions with ethylene. *J. Phys. B: At., Mol. Opt. Phys.* **2003**, *36*, 1615.
- (206) Szmytkowski, C.; Kwitniewski, S.; Ptasińska Denga, E. d. z. Electron collisions with tetrafluoroethylene (c₂f₄) and ethylene (c₂h₄) molecules. *Phys. Rev. A* **2003**, *68*, 032715.
- (207) Allan, M.; Winstead, C.; McKoy, V. Electron scattering in ethene: Excitation of the α ³B_{1u} state elastic scattering, and vibrational excitation. *Phys. Rev. A* **2008**, *77*, 042715.
- (208) Khakoo, M. A.; Khakoo, S. M.; Sakaamini, A.; Hlousek, B. A.; Hargreaves, L. R.; Lee, J.; Murase, R. Low-energy elastic electron scattering from ethylene: Elastic scattering and vibrational excitation. *Phys. Rev. A* **2016**, *93*, 012710.
- (209) Burrow, P.; Michejda, J. Electron transmission study of the formaldehyde electron affinity. *Chem. Phys. Lett.* **1976**, *42*, 223–226.
- (210) Van Veen, E.; Van Dijk, W.; Brongersma, H. Low-energy electron-impact excitation spectra of formaldehyde, acetaldehyde and acetone. *Chem. Phys.* **1976**, *16*, 337–345.
- (211) Benoit, C.; Abouaf, R. Low-energy electron collisions with formaldehyde: interference phenomena in the differential vibrational excitation cross section. *Chem. Phys. Lett.* **1986**, *123*, 134–138.
- (212) Loos, P.-F.; Scemama, A.; Duchemin, I.; Jacquemin, D.; Blaese, X. Pros and Cons of the Bethe–Salpeter Formalism for Ground-State Energies. *J. Phys. Chem. Lett.* **2020**, *11*, 3536–3545.
- (213) Monino, E.; Loos, P.-F. Unphysical discontinuities, intruder states and regularization in GW methods. *J. Chem. Phys.* **2022**, *156*, 231101.
- (214) Burrow, P. D.; Sanche, L. Elastic Scattering of Low-Energy Electrons at 180° in CO₂. *Phys. Rev. Lett.* **1972**, *28*, 333–336.
- (215) Boness, M. J. W.; Schulz, G. J. Vibrational excitation in co₂ via the 3.8-eV resonance. *Phys. Rev. A* **1974**, *9*, 1969–1979.
- (216) Allan, M. Selectivity in the excitation of fermi-coupled vibrations in co₂ by impact of slow electrons. *Phys. Rev. Lett.* **2001**, *87*, 033201.
- (217) Lozano, A. I.; García-Abenza, A.; Blanco Ramos, F.; Hasan, M.; Slaughter, D. S.; Weber, T.; McEachran, R. P.; White, R. D.; Brunger, M. J.; Limão-Vieira, P.; García Gómez-Tejedor, G. Electron and Positron Scattering Cross Sections from CO₂: A Comparative Study over a Broad Energy Range (0.1–5000 eV). *J. Phys. Chem. A* **2022**, *126*, 6032–6046.
- (218) Bruneval, F.; Marques, M. A. L. Benchmarking the Starting Points of the GW Approximation for Molecules. *J. Chem. Theory Comput.* **2013**, *9*, 324–329.
- (219) Suhai, S. Quasiparticle energy-band structures in semiconducting polymers: Correlation effects on the band gap in polyacetylene. *Phys. Rev. B: Condens. Matter Mater. Phys.* **1983**, *27*, 3506–3518.
- (220) Holleboom, L. J.; Snijders, J. G. A Comparison between the Moller-Plesset and Green's Function Perturbative Approaches to the Calculation of the Correlation Energy in the Many-electron Problem. *J. Chem. Phys.* **1990**, *93*, 5826–5837.
- (221) Casida, M. E.; Chong, D. P. Physical interpretation and assessment of the Coulomb-hole and screened-exchange approximation for molecules. *Phys. Rev. A* **1989**, *40*, 4837–4848.
- (222) Casida, M. E.; Chong, D. P. Simplified Green-function approximations: Further assessment of a polarization model for second-order calculation of outer-valence ionization potentials in molecules. *Phys. Rev. A* **1991**, *44*, 5773–5783.
- (223) Stefanucci, G.; van Leeuwen, R. *Nonequilibrium Many-Body Theory of Quantum Systems: A Modern Introduction*; Cambridge University Press: Cambridge, 2013.
- (224) Ortiz, J. V. Electron propagator theory: An approach to prediction and interpretation in quantum chemistry: Electron propagator theory. *Wiley Interdiscip. Rev.: Comput. Mol. Sci.* **2013**, *3*, 123–142.
- (225) Phillips, J. J.; Zgid, D. Communication: The Description of Strong Correlation within Self-Consistent Green's Function Second-Order Perturbation Theory. *J. Chem. Phys.* **2014**, *140*, 241101.
- (226) Phillips, J. J.; Kananenka, A. A.; Zgid, D. Fractional Charge and Spin Errors in Self-Consistent Green's Function Theory. *J. Chem. Phys.* **2015**, *142*, 194108.
- (227) Rusakov, A. A.; Phillips, J. J.; Zgid, D. Local Hamiltonians for Quantitative Green's Function Embedding Methods. *J. Chem. Phys.* **2014**, *141*, 194105.
- (228) Rusakov, A. A.; Zgid, D. Self-Consistent Second-Order Green's Function Perturbation Theory for Periodic Systems. *J. Chem. Phys.* **2016**, *144*, 054106.
- (229) Hirata, S.; Hermes, M. R.; Simons, J.; Ortiz, J. V. General-Order Many-Body Green's Function Method. *J. Chem. Theory Comput.* **2015**, *11*, 1595–1606.
- (230) Hirata, S.; Doran, A. E.; Knowles, P. J.; Ortiz, J. V. One-particle many-body Green's function theory: Algebraic recursive

- definitions, linked-diagram theorem, irreducible-diagram theorem, and general-order algorithms. *J. Chem. Phys.* **2017**, *147*, 044108.
- (231) Backhouse, O. J.; Santana-Bonilla, A.; Booth, G. H. Scalable and predictive spectra of correlated molecules with moment truncated iterated perturbation theory. *J. Phys. Chem. Lett.* **2021**, *12*, 7650–7658.
- (232) Backhouse, O. J.; Booth, G. H. Efficient excitations and spectra within a perturbative renormalization approach. *J. Chem. Theory Comput.* **2020**, *16*, 6294–6304.
- (233) Backhouse, O. J.; Nusspickel, M.; Booth, G. H. Wave function perspective and efficient truncation of renormalized second-order perturbation theory. *J. Chem. Theory Comput.* **2020**, *16*, 1090–1104.
- (234) Pokhilko, P.; Zgid, D. Interpretation of multiple solutions in fully iterative GF2 and GW schemes using local analysis of two-particle density matrices. *J. Chem. Phys.* **2021**, *155*, 024101.
- (235) Pokhilko, P.; Iskakov, S.; Yeh, C.-N.; Zgid, D. Evaluation of two-particle properties within finite-temperature self-consistent one-particle Green's function methods: Theory and application to GW and GF2. *J. Chem. Phys.* **2021**, *155*, 024119.
- (236) Pokhilko, P.; Yeh, C.-N.; Zgid, D. Iterative subspace algorithms for finite-temperature solution of Dyson equation. *J. Chem. Phys.* **2022**, *156*, 094101.
- (237) Loos, P.-F.; Marie, A.; Ammar, A. Cumulant Green's function methods for molecules. *Faraday Discuss.* **2024**, *254*, 240–260.
- (238) Monino, E.; Loos, P.-F. Spin-conserved and spin-flip optical excitations from the bethe–salpeter equation formalism. *J. Chem. Theory Comput.* **2021**, *17*, 2852–2867.
- (239) Caruso, F.; Rinke, P.; Ren, X.; Scheffler, M.; Rubio, A. Unified description of ground and excited states of finite systems: The self-consistent GW approach. *Phys. Rev. B: Condens. Matter Mater. Phys.* **2012**, *86*, 081102.
- (240) Caruso, F.; Rinke, P.; Ren, X.; Rubio, A.; Scheffler, M. Self-consistent GW: All-electron implementation with localized basis functions. *Phys. Rev. B: Condens. Matter Mater. Phys.* **2013**, *88*, 075105.



CAS BIOFINDER DISCOVERY PLATFORM™

BRIDGE BIOLOGY AND CHEMISTRY FOR FASTER ANSWERS

Analyze target relationships,
compound effects, and disease
pathways

Explore the platform

